Shell-model study of Pb, Bi, Po, At, Rn, and Fr isotopes with masses from 210 to 217

K. Yanase,[1,*] E. Teruya,[1,†] K. Higashiyama,[2,‡] and N. Yoshinaga[1,§]
[1]*Department of Physics, Saitama University, Saitama City 338-8570, Japan*
[2]*Department of Physics, Chiba Institute of Technology, Narashino, Chiba 275-0023, Japan*

(Received 7 February 2018; revised manuscript received 29 May 2018; published 5 July 2018)

Large-scale shell-model calculations are performed for even-even, odd-mass, and doubly odd nuclei of Pb, Bi, Po, At, Rn, and Fr isotopes in the neutron rich region ($N > 126$) assuming ^{208}Pb as a doubly magic core. Seven orbitals above the magic number 126, the $1g_{9/2}$, $0i_{11/2}$, $0j_{15/2}$, $2d_{5/2}$, $3s_{1/2}$, $1g_{7/2}$, and $2d_{3/2}$ orbitals, are considered for neutrons and all the six orbitals between the magic numbers 82 and 126, the $0h_{9/2}$, $1f_{7/2}$, $0i_{13/2}$, $2p_{3/2}$, $1f_{5/2}$, and $2p_{1/2}$ orbitals, are considered for protons. For a phenomenological effective two-body interaction, one set of the monopole-pairing, quadrupole-quadrupole, and multipole-pairing interactions is adopted for all the nuclei considered. The calculated energies and electromagnetic properties are compared with the experimental data. Many isomeric states are analyzed in terms of the shell-model configurations. The spins and parities of some experimentally ambiguous states are suggested.

DOI: 10.1103/PhysRevC.98.014308

I. INTRODUCTION

Structure of heavy nuclei has not been studied enough compared to that of light nuclei. Recent experimental situation on some of heavy nuclei ($Z \geqslant 82$, $N > 126$) is as follows. The ^{212}Bi nucleus was studied using a ^{238}U beam, and two isomers with long half-lives of 25 min and 7 min were confirmed [1]. However, the number of observed states in this nucleus is limited so that the spins and parities of only a few states are assigned. The level structure of ^{213}Po was studied through the $^{18}\mathrm{O} + {}^{208}$Pb reaction using the γ multidetector array [2]. The level scheme was built up to about 2 MeV of excitation energy and spins were assigned up to 25/2 using the triple γ coincidence data. The constructed level scheme was compared with an empirical shell-model calculation. The ^{211}Pb nucleus was studied through the deep-inelastic reactions between a beam of ^{208}Pb ions and a ^{238}U target [3]. Spins and parities of high-spin states including three high-spin isomers were identified. Configurations of several states were assigned by comparing them with a shell-model calculation using empirical interactions. High-spin states of ^{210}Pb and ^{211}Bi were studied using deep-inelastic collisions of a pulsed beam of ^{208}Pb ions on a ^{238}U target [4]. Configurations of some isomers were discussed and analyzed.

Nuclei with a few valence nucleons have been studied theoretically using the shell-model approach. The ^{210}Bi nucleus is a system with one valence neutron and one valence proton outside the doubly magic core ^{208}Pb and it is relatively easy to analyze theoretically [5–9]. It is an intriguing nucleus to study the interaction between a neutron and a proton. One of the theoretical problems on this nucleus is associated with the fact that the spin-parity of the experimental ground state is 1^- with the $(\nu g_{9/2} \otimes \pi h_{9/2})$ configuration. The 0^-, 1^-, ..., 9^- states with the $(\nu g_{9/2} \otimes \pi h_{9/2})$ configuration are observed in this nucleus. From the Nordheim strong coupling rule [9,10], the 0^- state should be the lowest among the states with the $(\nu g_{9/2} \otimes \pi h_{9/2})$ configuration. However, as mentioned, the experimental observation is different from this theoretical prediction. It was concluded in theoretical studies using empirical two-body interactions that tensor-force components are necessary to reproduce the ground state [5–7].

Recently, precise calculations employing the interaction delivered from the NN potential were performed and good agreements with the experimental data were obtained [9]. The $(\pi h_{9/2} \otimes \nu g_{9/2})$, $(\pi f_{7/2} \otimes \nu i_{11/2})$, $(\pi h_{9/2} \otimes \nu i_{11/2})$, $(\pi f_{7/2} \otimes \nu g_{9/2})$, and $(\pi h_{9/2} \otimes \nu j_{15/2})$ configurations in the low-lying states of ^{210}Bi, ^{212}Bi, ^{212}At, ^{216}At, and ^{216}Fr were compared with the experimental results [11]. The structure of the low-lying states and transition rates of ^{210}Pb and ^{210}Bi were calculated using a conventional shell-model approach with a central Gaussian-shaped interaction [12]. Although orders of energy levels of several states were reversely predicted, transition rates and $M1$-$E2$ branching ratios were well reproduced.

In the previous paper [13], even-even, odd-mass, and doubly odd nuclei for $_{82}$Pb, $_{83}$Bi, $_{84}$Po, $_{85}$At, $_{86}$Rn, and $_{87}$Fr isotopes with neutrons less than 126 were calculated. In that work 33 nuclei were analyzed using the large-scale shell model. Good agreements with the experimental data were obtained.

In this paper, the isotopes with neutrons larger than 126, and with up to four valence neutrons are considered assuming ^{208}Pb as a doubly magic core. Energy spectra and electromagnetic properties are calculated and compared with the experimental data. Isomeric states are analyzed in terms of the shell-model configurations. As shown above, some nuclei in this mass region have been analyzed theoretically. However, in most

*yanase@nuclei.th.phy.saitama-u.ac.jp
†teruya@nuclei.th.phy.saitama-u.ac.jp
‡koji.higashiyama@it-chiba.ac.jp
§yoshinaga@phy.saitama-u.ac.jp

studies only a few nuclei are considered and there are no systematic calculations in this mass region.

This paper is organized as follows. The general framework of the present shell-model study is given in Sec. II. Energy spectra and electromagnetic properties are presented and compared with the experimental data for each nucleus in Sec. III. Some characteristic features on even-even nuclei in this mass region are analyzed and discussed in Sec. IV. Finally, this work is summarized in Sec. V.

II. THEORETICAL FRAMEWORK

Systematic studies are carried out for even-even, odd-mass, and doubly odd nuclei around the double-magic ^{208}Pb nucleus using a shell-model framework. For neutron single-particle levels, seven orbitals above the magic number 126, the $1g_{9/2}$, $0i_{11/2}$, $0j_{15/2}$, $2d_{5/2}$, $3s_{1/2}$, $1g_{7/2}$, and $2d_{3/2}$ orbitals, are taken into account. For proton single-particle levels, all the six orbitals in the major shell between the magic numbers 82 and 126, $0h_{9/2}$, $1f_{7/2}$, $0i_{13/2}$, $2p_{3/2}$, $1f_{5/2}$, and $2p_{1/2}$ orbitals, are taken into account.

The single-particle energies $\varepsilon_\tau(\tau = \nu \text{ or } \pi)$ employed in the present calculations are listed in Table I, which are extracted from the experimental energy levels of ^{209}Bi (for proton single-particle energies) and ^{209}Pb (for neutron single-particle energies). As for the neutron $0j_{15/2}$ and $0i_{11/2}$ orbitals and the proton $0i_{13/2}$ and $1f_{7/2}$ orbitals, the single-particle energies are assumed to be changed linearly with the numbers of valence neutrons and protons. They are determined in units of MeV as follows:

$$\epsilon_\nu(j_{15/2}) = -0.050N_\nu - 0.160N_\pi + 1.473, \quad (1)$$

$$\epsilon_\nu(i_{11/2}) = -0.070N_\nu - 0.050N_\pi + 0.849, \quad (2)$$

$$\epsilon_\pi(i_{13/2}) = -0.050N_\pi + 1.659, \quad (3)$$

$$\epsilon_\pi(f_{7/2}) = -0.170N_\nu + 0.050N_\pi + 0.846, \quad (4)$$

where N_ν and N_π represent the numbers of valence neutrons and valence protons, respectively. The number dependence is introduced for a better reproduction of the low-lying states of odd-mass nuclei.

As an effective interaction, an extended pairing plus quadrupole-quadrupole interaction is employed. The effective shell-model Hamiltonian is given by

$$\hat{H} = \hat{H}_\nu + \hat{H}_\pi + \hat{H}_{\nu\pi}, \quad (5)$$

TABLE I. Adopted single-particle energies ε_τ for neutrons ($\tau = \nu$) and protons ($\tau = \pi$) in units of MeV. The single-particle energies for the neutron $0j_{15/2}$ and $0i_{11/2}$ orbitals and the proton $0i_{13/2}$ and $1f_{7/2}$ orbitals are changed linearly with the numbers of valence neutrons (N_ν) and valence protons (N_π). Definitions of $\epsilon_\nu(j_{15/2})$, $\epsilon_\nu(i_{11/2})$, $\epsilon_\pi(i_{13/2})$, and $\epsilon_\pi(f_{7/2})$ are given in the text.

j	$1g_{9/2}$	$0i_{11/2}$	$0j_{15/2}$	$2d_{5/2}$	$3s_{1/2}$	$1g_{7/2}$	$2d_{3/2}$
ε_ν	0.000	$\epsilon_\nu(i_{11/2})$	$\epsilon_\nu(j_{15/2})$	1.567	2.032	2.491	2.538
j	$0h_{9/2}$	$1f_{7/2}$	$0i_{13/2}$	$2p_{3/2}$	$1f_{5/2}$	$2p_{1/2}$	
ε_π	0.000	$\epsilon_\pi(f_{7/2})$	$\epsilon_\pi(i_{13/2})$	3.119	2.826	3.634	

TABLE II. Strengths of adopted two-body interactions between neutrons (ν-ν) and those between protons (π-π). G_0 and G_2 indicate the strengths of the monopole (MP) and quadrupole-pairing (QP) interactions, respectively. G_L ($L = 4,6,8,10$) denote the strengths for higher multipole-pairing (HMP) interactions. The strengths of the MP and HMP interactions are given in units of MeV. The strengths of the QP interactions are given in units of MeV/b^4, where b is the oscillator parameter.

	G_0	G_2	G_4	G_6	G_8	G_{10}
ν-ν	0.102	0.008	0.425	0.500	0.500	0.450
π-π	0.145	0.013	0.400	0.400	−0.600	0.000

where $\hat{H}_\nu$, $\hat{H}_\pi$, and $\hat{H}_{\nu\pi}$ represent neutron, proton, and neutron-proton interactions, respectively. The interactions among like nucleons are expressed as

$$\hat{H}_\tau = \hat{H}_{c\tau} + \hat{H}_{h\tau}. \quad (6)$$

The first term $\hat{H}_{c\tau}$ ($\tau = \nu$ or π) represents the conventional pairing interactions, which consist of spherical single-particle energies, the monopole-pairing (MP) interaction, and the quadrupole-pairing (QP) interaction,

$$\hat{H}_{c\tau} = \sum_{jm} \varepsilon_{j\tau} c^\dagger_{jm\tau} c_{jm\tau} - G_{0\tau} \hat{P}^{\dagger(0)}_\tau \hat{P}^{(0)}_\tau - G_{2\tau} \hat{P}^{\dagger(2)}_\tau \cdot \hat{\tilde{P}}^{(2)}_\tau. \quad (7)$$

The second term $\hat{H}_{h\tau}$ in Eq. (6) represents higher-order interactions, which consist of higher multipole-pairing (HMP) interactions,

$$\hat{H}_{h\tau} = -\sum_{L=4,6,8,10} G_{L\tau} \hat{P}^{\dagger(L)}_\tau \cdot \hat{\tilde{P}}^{(L)}_\tau. \quad (8)$$

The adopted two-body interaction strengths are listed in Table II. Only one set of strengths is adopted for all the nuclei considered. Detailed definitions of the interactions are given in Ref. [14].

Only for the proton part, an additional pairing interaction with spin 8 between two protons in the $0h_{9/2}$ and $1f_{7/2}$ orbitals (MP-8) is added to Eq. (6). It is explicitly defined as

$$\hat{H}^{(8)}(\pi h_{9/2} f_{7/2}) = -G^{(8)}_{\pi h_{9/2} f_{7/2}} \hat{P}^{\dagger(8)}_\pi(h_{9/2} f_{7/2}) \cdot \hat{\tilde{P}}^{(8)}_\pi(h_{9/2} f_{7/2}), \quad (9)$$

with

$$\hat{P}^{\dagger(8)}_{M\pi}(h_{9/2} f_{7/2}) = \left[c^\dagger_{h_{9/2}} c^\dagger_{f_{7/2}}\right]^{(8)}_M, \quad (10)$$

and the strength is taken as $G^{(8)}_{\pi h_{9/2} f_{7/2}} = 0.50$ MeV. Here, two protons in the $0h_{9/2}$ and $1f_{7/2}$ orbitals are coupled with spin 8, which is the maximum spin available between these two orbitals, and positive parity. $c^\dagger_j$ is the nucleon creation operator in the orbital j. The necessity of this interaction was discussed and its effects were analyzed in the previous paper [13].

The interaction between neutrons and protons $\hat{H}_{\nu\pi}$ consists of the quadrupole-quadrupole (QQ) interaction, which is given as

$$\hat{H}_{\nu\pi} = -\kappa_{\nu\pi} \hat{Q}_\nu \cdot \hat{Q}_\pi, \quad (11)$$

where the strength is taken as $\kappa_{\nu\pi} = 0.080\ \mathrm{MeV}/b^4$. Here harmonic-oscillator states are used as the single-particle basis states with the oscillator parameter $b = \sqrt{\hbar/M\omega}$.

The number occupancy v_j^2 is defined as

$$v_j^2 \equiv \langle \Psi(I_i^\pi) | \hat{n}_j | \Psi(I_i^\pi) \rangle, \tag{12}$$

where $\hat{n}_j$ is the number operator in the orbital j and $|\Psi(I_i^\pi)\rangle$ is the ith eigenstate with spin I and parity π of the Hamiltonian in Eq. (5) for a specific nucleus.

In this mass region, shell-model dimensions for diagonalization are too large to perform full calculations without truncation. Thus it is necessary to truncate the shell-model dimensions. In this study, the same truncation scheme adopted in Sec. II B of Ref. [14] is taken for all the nuclei. All calculations are performed with the truncation of $L_c = 500$. Here the definition of L_c is the same as given in Sec. II B in Ref. [14]. This truncation is found to be sufficient for reproducing low-lying energy levels and electromagnetic transitions among low-lying states after checking the effect of truncation by increasing $L_c = 500$ to $L_c = 1000$.

In this paper, $E2$ transition rates, magnetic moments, and quadrupole moments are also calculated. For $E2$ transition rates and quadrupole moments, the effective charges are taken as $e_\nu = 1.00e$ for neutrons and $e_\pi = 1.50e$ for protons. For magnetic moments, the gyromagnetic ratios of orbital angular momentum are taken as $g_{\ell\nu} = 0.00$ and $g_{\ell\pi} = 1.00$, and the gyromagnetic ratios of spin are taken as $g_{s\nu} = -2.87$ and $g_{s\pi} = 2.79$. These effective charges and gyromagnetic ratios are adjusted to reproduce the experimental data for single-closed nuclei on the whole. Further details of the electromagnetic transition operators are presented in Ref. [14].

III. NUMERICAL RESULTS

In this section, the results are given for each nucleus. Energy spectra, $E2$ transition rates, magnetic moments, and quadrupole moments are calculated. For energy spectra, up to four observed energy levels from the yrast state are shown for each spin-parity. As for the theoretical states, the two lowest energy levels are shown for each spin-parity in general.

A. Pb isotopes

Here $^{210-212}$Pb isotopes are discussed. Figure 1 shows the theoretical energy spectrum of ^{210}Pb in comparison with the experimental data [15,16]. The ^{210}Pb nucleus is a system with two valence neutrons outside the doubly magic core ^{208}Pb. This nucleus tells us information about the interactions between two neutrons. The calculation reproduces the yrast band well. In particular the narrow energy gap between the 4^+ and 6^+ states and that between the 6^+ and 8^+ states are well reproduced. The 6^+ and 8^+ states are isomers with half-lives of 49 ns and 201 ns, respectively [15]. The 2_1^+, 4_1^+, 6_1^+, and 8_1^+ states mainly consist of the $(\nu g_{9/2}^2)$ configuration, although the structure of the ground (0_1^+) state is not simple. In the ground state the occupation numbers (v_j^2) are 1.28, 0.35, and 0.21 for the neutron $1g_{9/2}$, $0i_{11/2}$, and $0j_{15/2}$ orbitals, respectively. The 10_1^+ state consists of the $(\nu g_{9/2} i_{11/2})$ configuration, which explains the large energy gap between the 8_1^+ and 10_1^+ states. The 12_1^+ and 14_1^+ states consist of the $(\nu j_{15/2}^2)$ configuration.

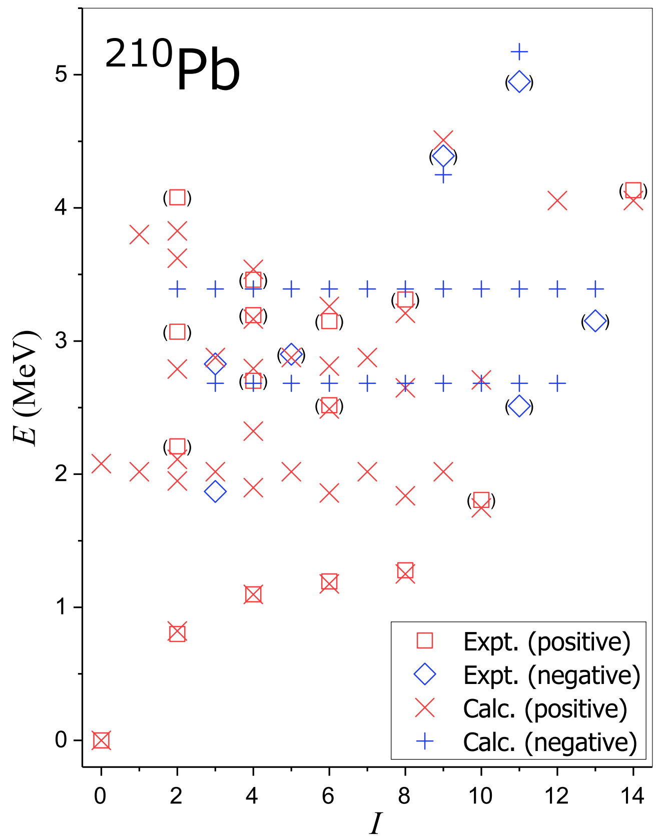

FIG. 1. The theoretical energy spectrum of ^{210}Pb (Calc.) in comparison with experimental data (Expt.). The experimental data are taken from Refs. [15,16]. The squares and diamonds represent experimental positive and negative parity states, respectively. The × marks and + marks represent theoretical positive and negative parity states, respectively.

Figure 2 shows the theoretical energy spectrum of ^{212}Pb in comparison with the experimental data [15,17]. In ^{212}Pb

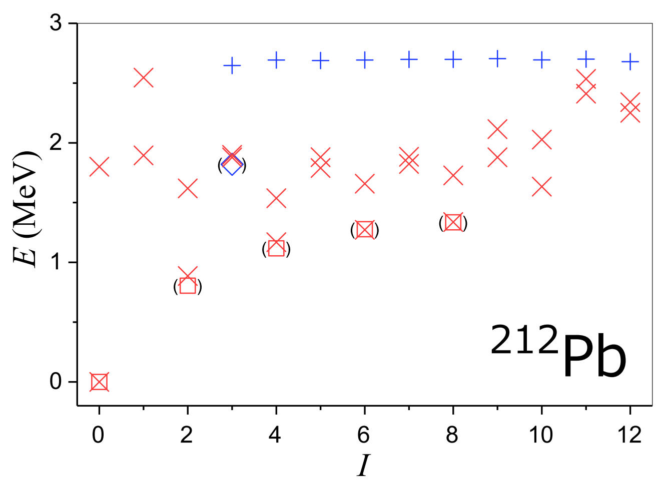

FIG. 2. Same as Fig. 1, but for ^{212}Pb. The experimental data are taken from Refs. [15,17].

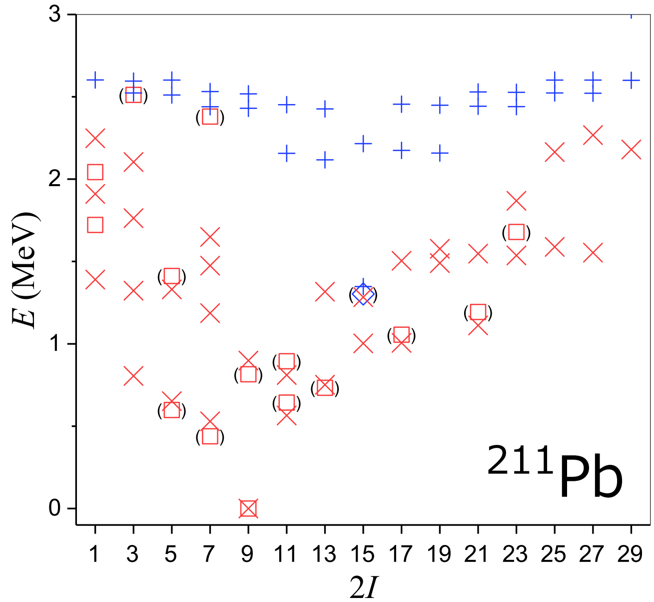

FIG. 3. Same as Fig. 1, but for ^{211}Pb. The experimental data are taken from Refs. [15,18].

the spins and parities of only several states are assigned in experiment. The yrast band up to spin 8 is well reproduced and the unobserved 10_1^+ state is calculated at 1.633 MeV. In ^{210}Pb and ^{212}Pb the almost degenerate 3_1^-, 4_1^-, ..., 12_1^- states are predicted at 2.682 MeV and around 2.69 MeV, respectively, in theory. However, the experimental 3_1^- states are located at 1.870 MeV and 1.820 MeV, respectively. These octupole one-phonon states are constructed by the particle-hole excitations [19,20], which are beyond the present shell-model framework. The low-lying 3^- states made by core excitations are also seen in Pb isotopes in the mass 210 region as discussed in Ref. [13].

Figure 3 shows the theoretical energy spectrum of ^{211}Pb in comparison with the experimental data [15,18]. Low-lying states are well reproduced. A $(27/2^+)$ state is observed at $1.679 + x$ MeV with x unknown and its half-life is 159 ns [15]. The $27/2_1^+$ state is calculated at 1.554 MeV and consists of the $(\nu g_{9/2}^2 i_{11/2})$ configuration, which is consistent with the result in Ref. [3]. The $(21/2^+)$ state observed at 1.193 MeV is also an isomer with a half-life of 42(7) ns and decays to the $(17/2^+)$ state observed at 1.056 MeV [15]. Both the initial and the final states consist of the $(\nu g_{9/2}^3)$ configuration in theory.

Calculated results for $B(E2)$ values and electromagnetic moments of Pb isotopes are given in Tables III and IV in comparison with the experimental data [3,15–18]. Most of the $B(E2)$ values are well reproduced in the calculation. The largest discrepancy between the experimental value and the theoretical one is seen in the $B(E2; 2_1^+ \to 0_1^+)$ value of ^{210}Pb. The calculated result is 2.2 times larger than the experimental one. The calculated $B(E2; 10_1^+ \to 8_1^+)$ values of ^{210}Pb and ^{212}Pb are much smaller than the other transition rates among the yrast states. The 8_1^+ state consists of two neutrons in the $1g_{9/2}$ orbital. However, one neutron needs to be excited to the $0i_{11/2}$ orbital to make the 10_1^+ state and the configuration is changed from the 8_1^+ state to the 10_1^+ state. The $E2$ transition rate from

TABLE III. The calculated $B(E2)$ values in units of W.u. for Pb isotopes (Calc.) in comparison with the experimental data (Expt.) [3,15–18].

^{210}Pb	$B(E2)$ Expt.	$B(E2)$ Calc.
$2_1^+ \to 0_1^+$	1.4(4)	3.130
$4_1^+ \to 2_1^+$	4.8(9)	3.435
$6_1^+ \to 4_1^+$	2.1(8)	2.450
$8_1^+ \to 6_1^+$	0.7(3)	1.056
$10_1^+ \to 8_1^+$		0.154
^{212}Pb	Expt.	Calc.
$2_1^+ \to 0_1^+$		5.535
$4_1^+ \to 2_1^+$		1.353
$6_1^+ \to 4_1^+$		0.766
$8_1^+ \to 6_1^+$		0.303
$10_1^+ \to 8_1^+$		0.186
^{211}Pb	Expt.	Calc.
$5/2_1^+ \to 9/2_1^+$		2.870
$7/2_1^+ \to 9/2_1^+$		4.924
$11/2_1^+ \to 9/2_1^+$		0.052
$13/2_1^+ \to 9/2_1^+$		3.125
$21/2_1^+ \to 17/2_1^+$	1.36(23)	2.290
$27/2_1^+ \to 23/2_1^+$	1.0^{+2}_{-3}[a]	1.583

[a]Using theoretical transition energy of 29 keV [3].

TABLE IV. The results of magnetic dipole moments μ in units of μ_N and electric quadrupole moments Q in units of eb for Pb isotopes (Calc.) in comparison with the experimental data (Expt.) [15–18].

^{210}Pb	μ Expt.	μ Calc.	Q Expt.	Q Calc.
2_1^+		−0.343		+0.016
4_1^+		−0.969		+0.015
6_1^+	−1.872(90)	−1.602		−0.137
8_1^+	−2.496(64)	−2.360		−0.433
10_1^+		−0.207		−0.677
^{212}Pb	Expt.	Calc.	Expt.	Calc.
2_1^+		−0.316		−0.123
4_1^+		−0.894		−0.086
6_1^+		−1.469		−0.093
8_1^+		−2.182		−0.176
10_1^+		−0.187		−0.511
^{211}Pb	Expt.	Calc.	Expt.	Calc.
$5/2_1^+$		−0.842		−0.040
$7/2_1^+$		−1.095		−0.332
$9/2_1^+$	−1.4037(8)	−1.380	+0.087(62)	−0.177
$11/2_1^+$		+1.167		−0.338
$13/2_1^+$		−1.658		−0.228

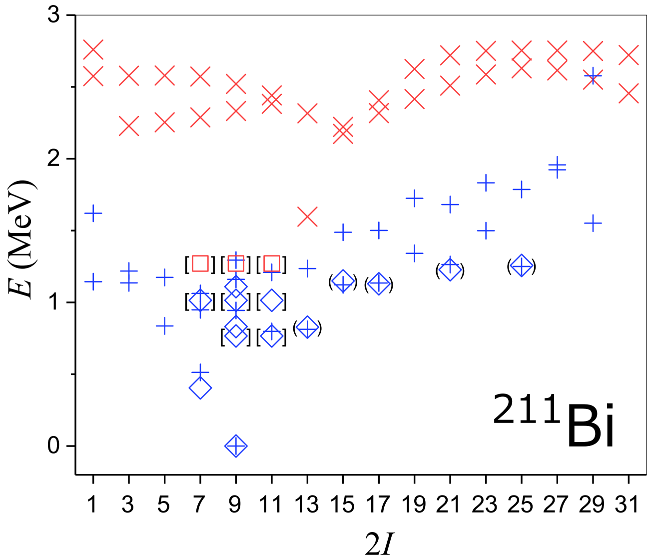

FIG. 4. Same as Fig. 1, but for ^{211}Bi. The experimental data are taken from Refs. [15,21]. Each ambiguous state with only one possible set of spin-parity in experiment is shown with parentheses, while each ambiguous state with more than two possible sets of spin-parity is shown separately with square bracket.

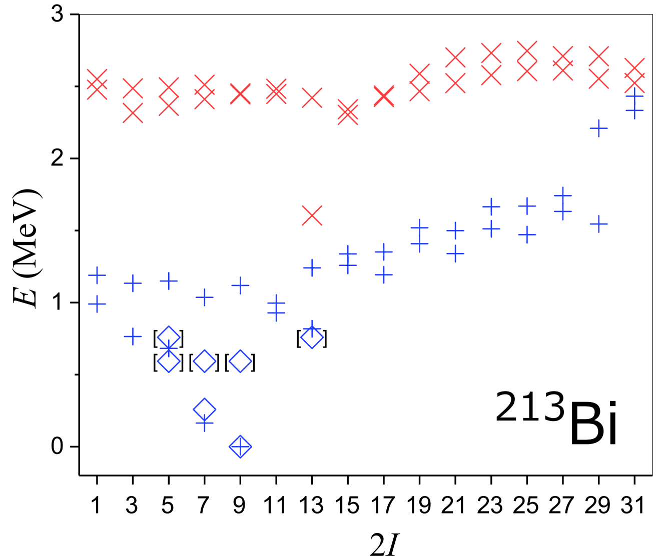

FIG. 5. Same as Fig. 4, but for ^{213}Bi. The experimental data are taken from Refs. [15,18].

the isomeric $21/2_1^+$ state to the $17/2_1^+$ state, $B(E2; 21/2_1^+ \to 17/2_1^+)$, is well reproduced. For the quadrupole moment of the $9/2_1^+$ state in ^{211}Pb, the experimental value (0.087) has a large error (0.062). Thus at the moment we cannot have any definite conclusion about the discrepancy between the theoretical value and the experimental one.

B. Bi isotopes

Here $^{210-213}$Bi isotopes are discussed. Figure 4 shows the theoretical energy spectrum of ^{211}Bi in comparison with the experimental data [15,18]. Low-lying negative parity states are well reproduced. The $(25/2^-)$ state observed at 1.257 MeV is an isomer with a half-life of 1.4 μs and decays to the $(21/2^-)$ state at 1.227 MeV by the $E2$ transition [15]. Both the $25/2_1^-$ and $21/2_1^-$ states consist of the $(\nu g_{9/2}^2 \otimes \pi h_{9/2})$ configuration. In the $25/2_1^-$ state, two neutrons in the $1g_{9/2}$ orbital are stretched to have spin 8. The maximum spin in the $(\nu g_{9/2}^2 \otimes \pi h_{9/2})$ configuration is 25/2. The spin-parity of the state observed at 0.767 MeV is assigned as $(9/2, 11/2)^-$. The theoretical $9/2_2^-$ and $11/2_1^-$ states are predicted at 0.944 MeV and 0.799 MeV, respectively. Thus the spin-parity of this ambiguous state is suggested to be $11/2^-$.

Figure 5 shows the theoretical energy spectrum of ^{213}Bi in comparison with the experimental data [15,21]. In ^{213}Bi, only the $9/2_1^-$ and $7/2_1^-$ states are definitely assigned in experiment. The states observed at 0.593 MeV and 0.759 MeV are assigned as $(5/2, 7/2, 9/2)^-$ and $(5/2^-, 13/2^-)$, respectively. The $5/2_1^-$ and $13/2_1^-$ states are calculated at 0.682 and 0.818 MeV, respectively. Thus it is inferred that the states at 0.593 MeV and 0.759 MeV are spin-parity $5/2^-$ and $13/2^-$, respectively.

Figure 6 shows the theoretical energy spectrum of ^{210}Bi in comparison with the experimental data [15,16]. The ^{210}Bi nucleus is a system with one neutron and one proton outside the doubly magic core ^{208}Pb. This nucleus tells us information on the interactions between neutrons and protons. The value

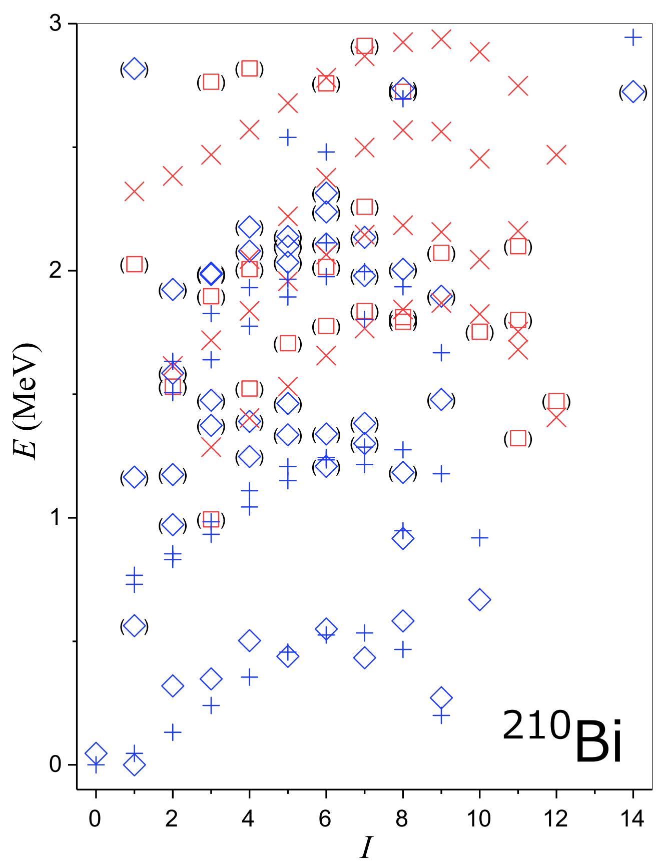

FIG. 6. Same as Fig. 1, but for ^{210}Bi. The experimental data are taken from Refs. [15,16].

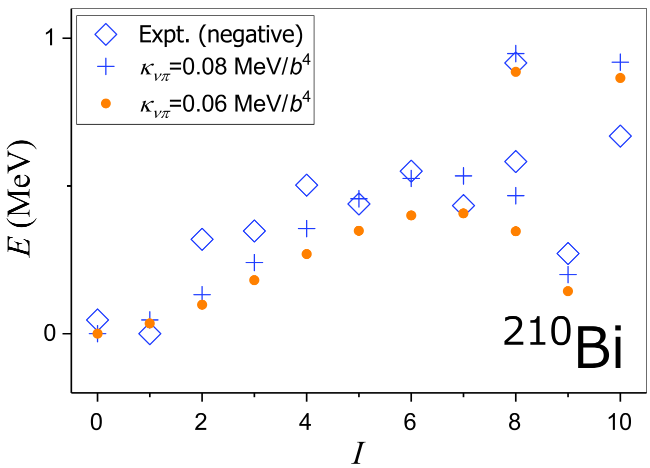

FIG. 7. Comparison of the low-lying energy levels of ^{210}Bi with those by the strength parameter $\kappa_{\nu\pi} = 0.06$ MeV/b^4, which are indicated by the filled circles. This value of $\kappa_{\nu\pi} = 0.06$ MeV/b^4 is the same in magnitude as used in Ref. [13].

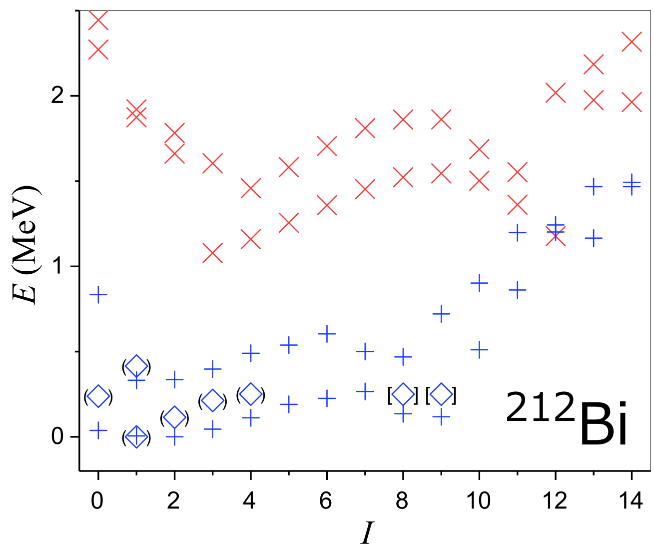

FIG. 8. Same as Fig. 4, but for ^{212}Bi. The experimental data are taken from Refs. [15,17].

of the strength parameter $\kappa_{\nu\pi} = 0.08$ MeV/b^4 adopted in the present study is slightly larger in magnitude than $\kappa_{\nu\pi} = -0.06$ MeV/b^4, which had been throughout used for nuclei with neutrons less than 126 and protons more than 82 [13]. The energy spectra for low-lying states of ^{210}Bi are compared with two choices of $\kappa_{\nu\pi}$ in Fig. 7. As seen in the figure, the experimental spectra are better reproduced with the strength of $\kappa_{\nu\pi} = 0.08$ MeV/b^4.

The spin-parity of the ground state is 1^- in experiment. From the Nordheim strong coupling rule [9,10], the 0^- state should be the lowest among the states with the $(\nu g_{9/2} \otimes \pi h_{9/2})$ configuration. However, the 0_1^-, 1_1^-, ..., 8_1^- states with the $(\nu g_{9/2} \otimes \pi h_{9/2})$ configuration are as a whole well described in our calculation. Thus it is suggested that the quadrupole-quadrupole interaction between the neutron and the proton is the main part of the interaction, although some tensor-force components might be necessary to reproduce the ground state. In our calculation the $1_2^-, 2_3^-, 3_3^-, 4_3^-, 5_3^-, 6_3^-, 7_2^-$, and 8_2^- states consist of the $(\nu g_{9/2} \otimes \pi f_{7/2})$ configuration, whereas the 1_3^-, $2_2^-, 3_2^-, 4_2^-, 5_2^-, 6_2^-, 7_3^-, 8_3^-, 9_2^-$, and 10_1^- states consist of the $(\nu i_{11/2} \otimes \pi h_{9/2})$ configuration.

Figure 8 shows the theoretical energy spectrum of ^{212}Bi in comparison with the experimental data [15,17]. In ^{212}Bi negative parity states are densely observed and calculated below 0.5 MeV. In theory the spin-parity of the ground state is 2^-. The lowest members of the $0_1^-, 1_1^-, \cdots, 9_1^-$ states mainly consist of the $(\nu g_{9/2}^2 i_{11/2} \otimes \pi h_{9/2})$ configuration in our calculation, whereas the second lowest members of the $1_2^-, 2_2^-, \ldots, 8_2^-$ states mainly consist of the $(\nu g_{9/2}^2 i_{11/2} \otimes \pi f_{7/2})$ configuration. Positive parity states are calculated above 1.0 MeV.

Calculated results for $B(E2)$ values and electromagnetic moments of Bi isotopes are given in Tables V and VI in comparison with the experimental data [15–18,21]. As for $B(E2)$ transition rates, experimental data are given only for ^{211}Bi. The calculated $B(E2)$ value from the isomeric $25/2_1^-$ state to the $21/2_1^-$ state, $B(E2; 25/2_1^- \to 21/2_1^-)$, is 2.533 W.u. The long half-life of $25/2_1^-$ state is caused by the small energy gap between the $21/2_1^-$ and the $25/2_1^-$ states. Most of experimental values for the electromagnetic moments are well reproduced. However, the small experimental value of the magnetic moment for the 1_1^- state of ^{210}Bi is hardly reproduced without precisely adjusting the gyromagnetic ratios.

TABLE V. Same as Table III, but for Bi isotopes. The experimental data are taken from Refs. [15–18,21].

^{211}Bi	$B(E2)$	
	Expt.	Calc.
$7/2_1^- \to 9/2_1^-$	1.07(10)	0.624
$9/2_2^- \to 7/2_1^-$	>0.00015	0.392
$9/2_2^- \to 9/2_1^-$	>0.0031	0.747
$11/2_1^- \to 9/2_1^-$		3.405
$13/2_1^- \to 9/2_1^-$		3.984
$21/2_1^- \to 17/2_1^-$	1.44(11)	4.682
$25/2_1^- \to 21/2_1^-$		2.533
^{213}Bi	Expt.	Calc.
$7/2_1^- \to 9/2_1^-$		0.857
$9/2_2^- \to 7/2_1^-$		4.276
$9/2_2^- \to 9/2_1^-$		0.807
$11/2_1^- \to 9/2_1^-$		3.417
$13/2_1^- \to 9/2_1^-$		8.816
^{210}Bi	Expt.	Calc.
$3_1^- \to 1_1^-$		3.489
$3_1^- \to 2_1^-$		0.015
$0_1^- \to 2_1^-$		14.438
^{212}Bi	Expt.	Calc.
$3_1^- \to 2_1^-$		1.905
$0_1^- \to 2_1^-$		7.964

TABLE VI. Same as Table IV, but for Bi isotopes. The experimental data are taken from Refs. [15–18,21].

^{211}Bi	μ		Q	
	Expt.	Calc.	Expt.	Calc.
$7/2_1^-$	+4.5(7)	+4.147		−0.623
$9/2_1^-$	(+)3.79(7)	+3.647		−0.687
$11/2_1^-$		+2.698		−0.463
$13/2_1^-$		+2.978		−0.559
^{213}Bi	Expt.	Calc.	Expt.	Calc.
$7/2_1^-$		+4.095		−0.778
$9/2_1^-$	+3.717(13)	+3.584	−0.60(5)	−0.853
$11/2_1^-$		+3.325		−0.775
$13/2_1^-$		+3.218		−0.880
^{210}Bi	Expt.	Calc.	Expt.	Calc.
1_1^-	−0.04451(6)	+0.218	+0.136(1)	+0.199
5_1^-	+1.530(45)	+1.286		−0.034
7_1^-	+2.114(49)	+1.834		−0.349
9_1^-	2.728(42)	+2.336	−0.471(59)	−0.754
^{212}Bi	Expt.	Calc.	Expt.	Calc.
1_1^-	0.41(5)	+0.457	0.1(3)	+0.144
2_1^-		+0.734		+0.253
3_1^-		+0.880		+0.261
5_1^-		+1.276		−0.025
7_1^-		+1.792		−0.440
9_1^-		+2.286		−0.796

C. Po isotopes

Here $^{211-214}$Po isotopes are discussed. Figure 9 shows the theoretical energy spectrum of ^{212}Po in comparison with the experimental data [15,17]. The ^{212}Po nucleus is a system with two valence neutrons and two valence protons. The narrow energy gap between the yrast 6^+ and 8^+ states is well reproduced. The $0_1^+, 2_1^+, \ldots, 8_1^+$ states mainly consist of the $(\nu g_{9/2}^2 \otimes \pi(h_{9/2}^2)_{0^+})$ configuration. In contrast, the 10_1^+ state consists of the $[\nu g_{9/2} i_{11/2} \otimes \pi(h_{9/2}^2)_{0^+}]$ configuration. The 12_1^+ and 14_1^+ states consist of the $[\nu g_{9/2}^2 \otimes \pi(h_{9/2}^2)_{L^+}]$ configuration with L greater than zero. These structures are analyzed in Sec. IV.

In recent years, negative parity states have been experimentally observed below 2.5 MeV [22,23]. The observed 4^-, 6^-, and 8^- states are strongly connected to the yrast 4^+, 6^+, and 8^+ states by the $E1$ transitions, respectively. In Ref. [25], it was suggested that these negative parity states are constructed by the α particle coupled to 3^- states of ^{208}Pb [the coupled-channels of $\alpha + {}^{208}\mathrm{Pb}(3_1^-)$]. Another description of these states was suggested in Ref. [26]. They pointed out a possibility that these negative parity states consist of two-neutron excitations in ^{210}Pb coupled to the collective 3^- state in ^{208}Pb times ^{210}Po(g.s.) $(|[{}^{210}\mathrm{Pb}(J^+) \otimes {}^{210}\mathrm{Pb}(3^-)]_{I^-} \otimes {}^{210}\mathrm{Po(g.s.)}\rangle)$, where J and I represent angular momenta of states in ^{210}Pb and ^{212}Po, respectively. These negative parity states are out of the present shell-model framework.

The experimental (18^+) state at 2.922 MeV is an isomer with a half-life of 45.1(6) s [15], which mainly decays to the ground state, 3^- and 5^- states in ^{208}Pb by the α decay and partially decays to the (14^+) state at 2.885 MeV in ^{212}Po by the $E4$ transition. The configuration of the 18_1^+ state is $(\nu g_{9/2} i_{11/2} \otimes \pi h_{9/2}^2)$, which is in contrast with the $(\nu g_{9/2}^2 \otimes \pi h_{9/2}^2)$ configuration of the 14_1^+ and the 16_1^+ states. The theoretical energy of the 16_1^+ state is lower than the energy of the 18_1^+ state so that the 18_1^+ state can easily decay to the 16_1^+ state by the $E2$ transition. Therefore we cannot explain the long half-life of the (18^+) state. In order to achieve the situation that the 18_1^+ state decays to the 14_1^+ state rather

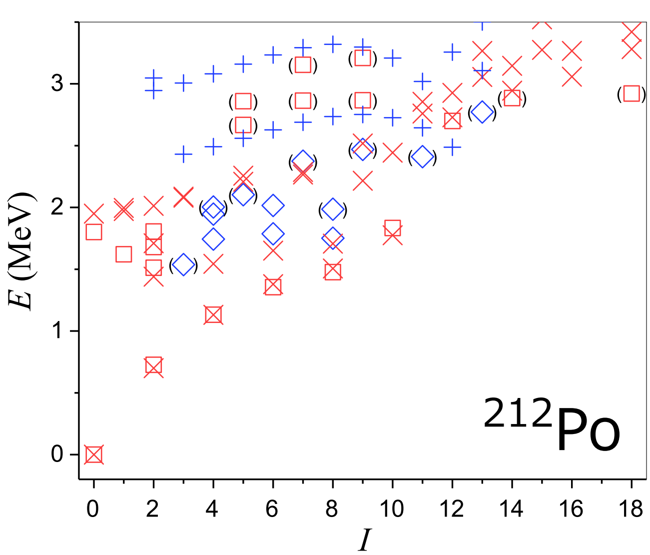

FIG. 9. Same as Fig. 1, but for ^{212}Po. The state at 1.249 MeV is not shown in the figure since the spin-parity is not assigned in experiment. The experimental data are taken from Refs. [15,17,22,23].

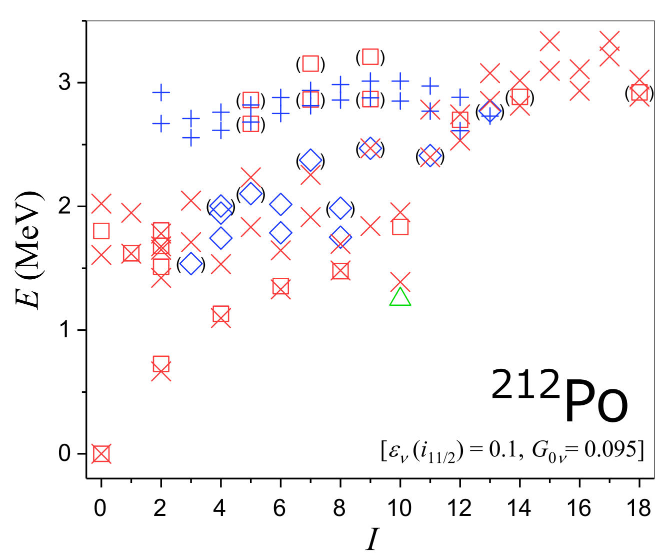

FIG. 10. Same as Fig. 9, but with $\varepsilon_\nu(i_{11/2}) = 0.1$ MeV and $G_{0\nu} = 0.095$ MeV. The spin-parity of the state at 1.249 MeV indicated by a triangle is not assigned in experiment, but it is suggested to have a spin-parity of 10^+ in this calculation.

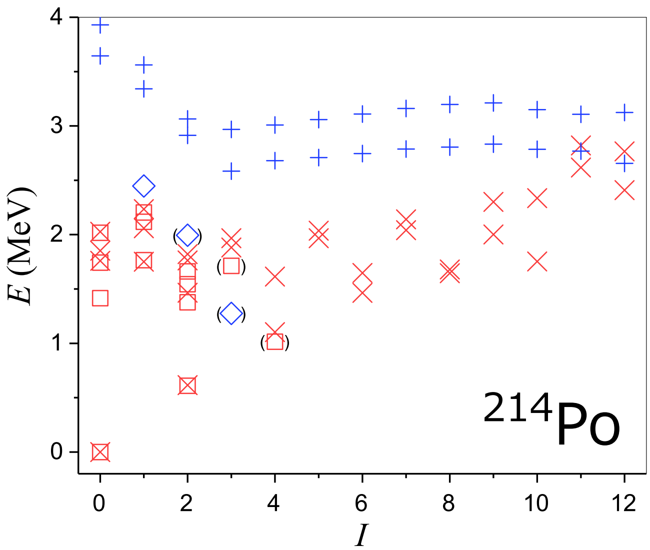

FIG. 11. Same as Fig. 1, but for ^{214}Po. The experimental data are taken from Refs. [15,24].

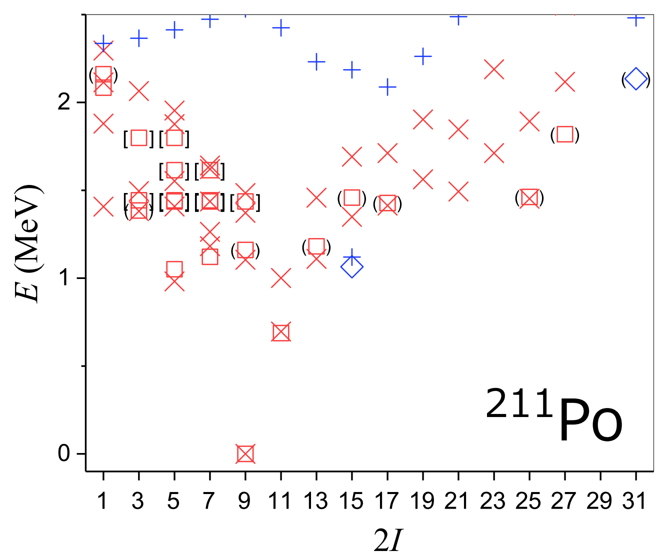

FIG. 12. Same as Fig. 4, but for ^{211}Po. The experimental data are taken from Refs. [15,18].

than the 16_1^+ state, we artificially lower the single-particle energy of the neutron $0i_{11/2}$ orbital as $\varepsilon_\nu(i_{11/2}) = 0.1$ MeV, and also reduce the strength of the monopole-pairing interaction between neutrons as $G_{0\nu} = 0.095$ MeV. The result is shown in Fig. 10. The spin-parity of the state observed at 1.249 MeV is not assigned, but theoretically it is suggested to have a spin-parity of 10^+. The calculation suggests that the (18^+) state at 2.922 MeV corresponds to the theoretical 18_1^+ state, while the unassigned state at 1.249 MeV and the 10^+ state at 1.833 MeV each corresponds to the 10_1^+ and the 10_2^+ states, respectively. We do not pursue this problem further, but the choice of the strengths of the interactions certainly affects the spectra of the neighboring nuclei and we need to investigate their effects on those nuclei. This is a problem for future research.

Figure 11 shows the theoretical energy spectrum of ^{214}Po in comparison with the experimental data [15,24]. In ^{214}Po, only the 0^+, 2^+, and 4^+ states are observed in the yrast band. The 6_1^+, 8_1^+, and 10_1^+ states are calculated at 1.465, 1.645, and 1.754 MeV, respectively. The state observed at 1.275 MeV is assigned as (3^-) [27]. The theoretical first 3_1^- state is calculated at 2.584 MeV. The experimental (3^-) state is supposed to be an octupole one-phonon state by the core excitation [27]. It is known in this mass region that the octupole correlation is crucial. The (2^-) state observed at 1.995 MeV is also considered to be a coupled state with the octupole and quadrupole phonon states. In our model space, all the negative parity states are calculated above 2.5 MeV.

Figure 12 shows the theoretical energy spectrum of ^{211}Po in comparison with the experimental data [15,18]. Low-lying states are well reproduced. The $25/2^+$ state observed at 1.462 MeV in ^{211}Po is an isomer with a half-life of 25.2(6) s [18]. This state decays to the $17/2^+$ state at 1.428 MeV by the $E4$ transition. The $25/2_1^+$ and $17/2^+$ states consist of the same configuration of $[\nu g_{9/2} \otimes \pi(h_{9/2}^2)_{L^+}]$ with $L = 8$ and $L = 4$, respectively. The $21/2_1^+$ and $23/2_1^+$ states, which are connected to the $25/2^+$ state by $E2$ or $M1$ transitions, are not observed. These states are calculated higher than the $25/2_1^+$ state. This isomer is classified as a spin-gap isomer.

Figure 13 shows the theoretical energy spectrum of ^{213}Po in comparison with the experimental data [2,15,21]. In ^{213}Po, only positive parity states are observed and well reproduced in our calculation. The lowest negative parity state, the $15/2_1^-$ state, is calculated at 1.017 MeV.

Calculated results for $B(E2)$ values and electromagnetic moments of Po isotopes are given in Tables VII and VIII in comparison with the experimental data [15,17,18,21,24,28,29]. In ^{212}Po, the calculated $B(E2; 2_1^+ \to 0_1^+)$ and $B(E2; 6_1^+ \to 4_1^+)$ values are much larger than the experimental data. In ^{213}Po, the theoretical calculation predicts large transition rates to the ground $(9/2_1^+)$ state from the $5/2_1^+$,

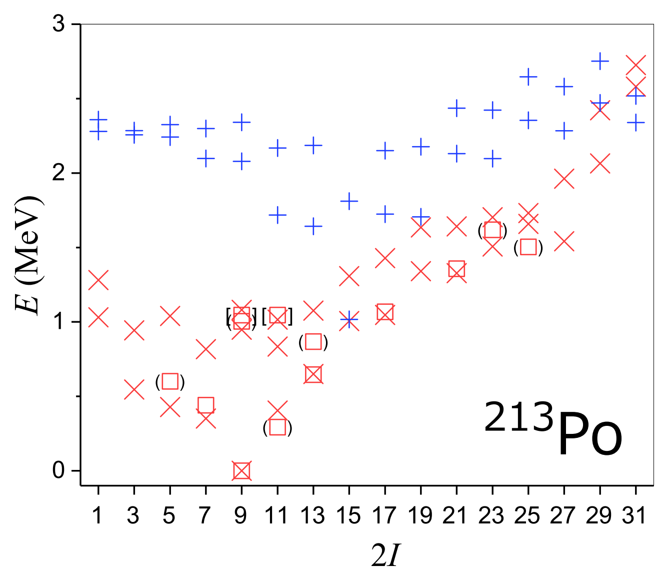

FIG. 13. Same as Fig. 4, but for ^{213}Po. The experimental data are taken from Refs. [2,15,21].

TABLE VII. Same as Table III, but for Po isotopes. The experimental data are taken from Refs. [15,17,18,21,24,28].

^{212}Po	$B(E2)$	
	Expt.	Calc.
$2_1^+ \to 0_1^+$	2.6(3)	10.921
$2_2^+ \to 0_1^+$	0.4(1)	0.246
$2_2^+ \to 2_1^+$	0.3(2)	1.843
$4_1^+ \to 2_1^+$		13.462
$6_1^+ \to 4_1^+$	3.9(11)	11.047
$8_1^+ \to 6_1^+$	2.30(9)	5.820
$10_1^+ \to 8_1^+$	2.2(6)	1.280
^{214}Po	Expt.	Calc.
$2_1^+ \to 0_1^+$		18.451
$4_1^+ \to 2_1^+$		25.205
$6_1^+ \to 4_1^+$		20.832
$8_1^+ \to 6_1^+$		5.445
$10_1^+ \to 8_1^+$		0.000
$0_2^+ \to 2_1^+$	0.159(10)	0.352
^{211}Po	Expt.	Calc.
$5/2_1^+ \to 9/2_1^+$		10.189
$7/2_1^+ \to 9/2_1^+$		2.321
$9/2_2^+ \to 9/2_1^+$		2.306
$11/2_1^+ \to 9/2_1^+$		0.403
$13/2_1^+ \to 9/2_1^+$		3.752
^{213}Po	Expt.	Calc.
$5/2_1^+ \to 9/2_1^+$		14.717
$7/2_1^+ \to 9/2_1^+$		13.168
$7/2_1^+ \to 11/2_1^+$		0.004
$11/2_1^+ \to 9/2_1^+$		0.282
$13/2_1^+ \to 9/2_1^+$		12.848

TABLE VIII. Same as Table IV, but for Po isotopes. The experimental data are taken from Refs. [15,17,18,21,24,29].

^{212}Po	μ		Q	
	Expt.	Calc.	Expt.	Calc.
2_1^+		+0.362		−0.070
4_1^+		+0.131		−0.198
6_1^+		−0.685		−0.423
8_1^+		−1.853		−0.769
10_1^+		−0.023		−1.141
^{214}Po	Expt.	Calc.	Expt.	Calc.
2_1^+		+0.454		−0.399
4_1^+		+0.751		−0.682
6_1^+		+0.753		−0.853
8_1^+		+7.319		−1.441
10_1^+		+0.049		−1.005
^{211}Po	Expt.	Calc.	Expt.	Calc.
$7/2_1^+$		−0.916		−0.501
$9/2_1^+$	−1.197(85)	−1.343	−0.77(8)	−0.591
$11/2_1^+$		+1.248		−0.623
$13/2_1^+$		+0.909		−0.357
$15/2_1^-$	−0.38(15)	−1.382		−0.764
^{213}Po	Expt.	Calc.	Expt.	Calc.
$7/2_1^+$		−0.936		−0.535
$9/2_1^+$		−1.251		−0.449
$11/2_1^+$		+1.230		−0.828
$13/2_1^+$		−0.856		−0.503

$7/2_1^+$, and $13/2_1^+$ states. In ^{211}Po, the magnetic moment of the $15/2_1^-$ state is largely predicted in magnitude by a factor of 3.6 compared with the experimental data, whereas the magnetic moment and the quadrupole moment of the ground ($9/2_1^+$) state are well reproduced. This discrepancy suggests that the $15/2_1^-$ state might be affected by the octupole excitation, namely the coupling of the ground ($9/2_1^+$) state with the octupole phonon state.

D. At isotopes

Here $^{212-215}$At isotopes are discussed. Figure 14 shows the theoretical energy spectrum of ^{213}At in comparison with the experimental data [15,21]. The spin-parity of the state observed at 0.341 MeV in ^{213}At is assigned as $(7/2^-,9/2^-)$. The $7/2_1^-$ and $9/2_2^-$ states are calculated at 0.348 and 0.958 MeV, respectively. Thus our calculation suggests that the spin-parity of this state is $7/2^-$.

Figure 15 shows the theoretical energy spectrum of ^{215}At in comparison with the experimental data [15,30]. The spin-parity of the state at 0.364 MeV in ^{215}At is assigned as $(13/2_1^+)$ [31]. However, the $13/2_1^+$ state is calculated at 1.332 MeV. Our calculation suggests that the spin-parity of the state is $3/2_1^-$ with the excitation energy of 0.402 MeV. A shell-model study by Liang and others suggested that the low-lying $9/2_1^-$, $5/2_1^-$, $7/2_2^-$, $13/2_1^-$, and $3/2_1^-$ states have the $(\nu g_{9/2}^4 \otimes \pi h_{9/2}^3)$ configuration [31]. However, it is shown in Table IX that these

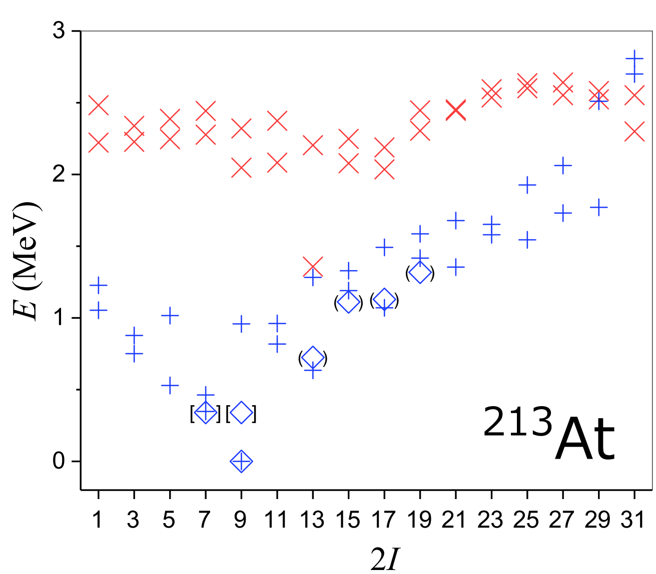

FIG. 14. Same as Fig. 4, but for ^{213}At. The experimental data are taken from Refs. [15,21].

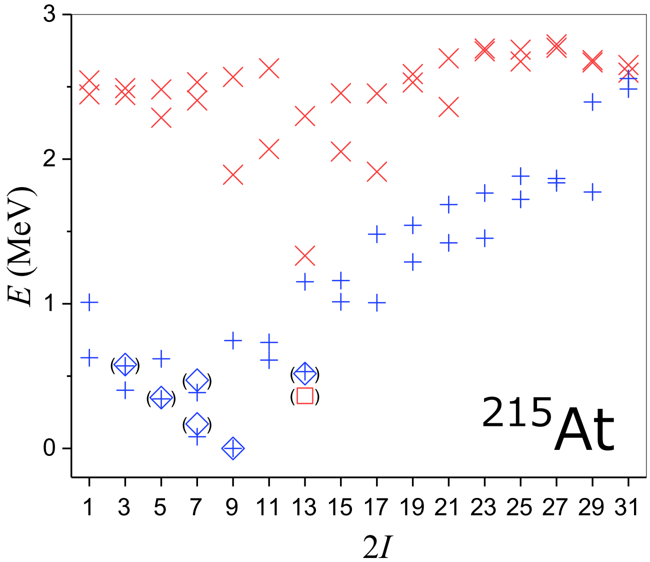

FIG. 15. Same as Fig. 1, but for ^{215}At. The experimental data are taken from Refs. [15,30].

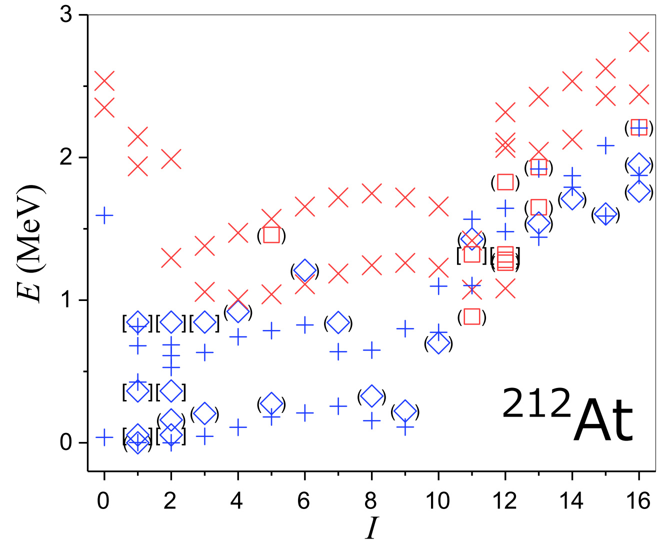

FIG. 16. Same as Fig. 4, but for ^{212}At. The experimental data are taken from Refs. [15,17].

states do not consist only of the neutron $1g_{9/2}$ and the proton $0h_{9/2}$ orbitals.

Figure 16 shows the theoretical energy spectrum of ^{212}At in comparison with the experimental data [15,17]. The (9^-) state at 0.223 MeV is an isomer with a half-life of 0.119(3) s [15]. The $0_1^-, 1_1^-, \ldots, 9_1^-$ states are members of the $(\nu g_{9/2} \otimes \pi h_{9/2}^3)$ configuration. The calculation reproduces the experimental situation such that the energy of the 9_1^- state is lower than that of the 8_1^- state. The members of the second negative parity band, the $1_2^-, 2_2^-, \ldots, 8_2^-$ states, consist of the $(\nu g_{9/2} \otimes \pi h_{9/2}^2 f_{7/2})$ configuration. The 11^+ state at 0.885 MeV is an isomer with a half-life of 18.7(7) ns and decays to the (10^-) state at 0.702 MeV by the $E1$ transition and the (9^-) state at 0.223 MeV by the $M2$ transition [15]. The 11_1^+ state mainly consists of the $(\nu j_{15/2} \otimes \pi h_{9/2}^3)$ configuration. The $6_1^+, 7_1^+, \ldots, 18_1^+$ states mainly consisting of the same configuration as the 11_1^+ state are located energetically higher than the 11_1^+ state.

Figure 17 shows the theoretical energy spectrum of ^{214}At in comparison with the experimental data [15,24]. In ^{214}At, only negative parity states are observed and densely located below 0.5 MeV. The $0_1^-, 1_1^-, \ldots, 9_1^-$ states consist of the $(\nu g_{9/2}^2 i_{11/2} \otimes \pi h_{9/2}^2 f_{7/2})$ configuration.

Calculated results for $B(E2)$ values and electromagnetic moments of At isotopes are given in Tables X and XI in comparison with the experimental data [15,17,21,24,30]. As for the $E2$ transitions, only two transition rates are measured in At isotopes. In ^{212}At, the experimental values of $B(E2; 5_1^- \to 3_1^-) = 3.3(3)$ W.u. and $B(E2; 15_1^- \to 13_1^-) = 3.1(3)$ W.u. are calculated as 4.715 W.u. and 4.295 W.u., respectively. As for electromagnetic moments, only the magnetic moments of the 15_1^- and 11_1^+ states in ^{212}At are observed. The magnetic moment of the 15_1^- state is 9.46(8) μ_N in experiment and the theoretical result is $+7.367\,\mu_N$, which is a reasonable value. The magnetic moment of the 11_1^+ state is 5.94(11)

TABLE IX. Occupation numbers in some low-lying states of ^{215}At.

ν	$1g_{9/2}$	$0i_{11/2}$	$0j_{15/2}$	$2d_{5/2}$	$3s_{1/2}$	$1g_{7/2}$	$2d_{3/2}$
$9/2_1^-$	2.06	0.99	0.61	0.16	0.03	0.09	0.05
$5/2_1^-$	2.17	0.95	0.52	0.18	0.03	0.09	0.05
$7/2_1^-$	2.08	0.98	0.60	0.16	0.03	0.09	0.05
$13/2_1^+$	2.21	0.94	0.50	0.18	0.03	0.09	0.05
π	$0h_{9/2}$	$1f_{7/2}$	$0i_{13/2}$	$2p_{3/2}$	$1f_{5/2}$	$2p_{1/2}$	
$9/2_1^-$	2.11	0.59	0.18	0.08	0.03	0.01	
$5/2_1^-$	2.10	0.55	0.16	0.13	0.05	0.01	
$7/2_1^-$	1.50	1.20	0.17	0.07	0.05	0.01	
$13/2_1^+$	2.12	0.58	0.16	0.09	0.04	0.01	

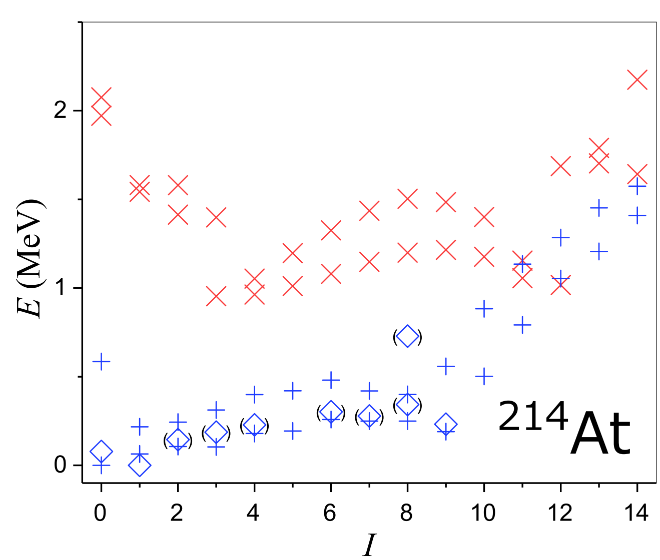

FIG. 17. Same as Fig. 1, but for ^{214}At. The experimental data are taken from Refs. [15,24].

TABLE X. Same as Table III, but for At isotopes. The experimental data are taken from Refs. [15,17,21,24,30].

^{213}At	$B(E2)$	
	Expt.	Calc.
$5/2^-_1 \to 9/2^-_1$		16.792
$7/2^-_1 \to 9/2^-_1$		4.474
$7/2^-_2 \to 9/2^-_1$		10.880
$13/2^-_1 \to 9/2^-_1$		14.392
$15/2^-_1 \to 13/2^-_1$		2.913
$17/2^-_1 \to 13/2^-_1$		18.147
$19/2^-_1 \to 17/2^-_1$		1.069
^{215}At	Expt.	Calc.
$5/2^-_1 \to 9/2^-_1$		33.195
$7/2^-_1 \to 9/2^-_1$		0.003
$7/2^-_2 \to 9/2^-_1$		18.121
$13/2^-_1 \to 9/2^-_1$		26.498
^{212}At	Expt.	Calc.
$5^-_1 \to 3^-_1$	3.3(3)	4.715
$8^-_1 \to 9^-_1$		2.079
$15^-_1 \to 13^-_1$	3.1(3)	4.295
^{214}At	Expt.	Calc.
$3^-_1 \to 1^-_1$		2.598
$5^-_1 \to 3^-_1$		8.861

TABLE XI. Same as Table IV, but for At isotopes. The experimental data are taken from Refs. [15,17,21,24,30].

^{213}At	μ		Q	
	Expt.	Calc.	Expt.	Calc.
$5/2^-_1$		+2.584		−0.131
$7/2^-_1$		+3.708		−0.777
$9/2^-_1$		+3.669		−0.480
$11/2^-_1$		+3.397		−0.354
$13/2^-_1$		+4.099		−0.533
$15/2^-_1$		+2.592		−0.595
$17/2^-_1$		+3.993		−0.625
$19/2^-_1$		+2.169		−0.786
^{215}At	Expt.	Calc.	Expt.	Calc.
$5/2^-_1$		2.484		−0.413
$7/2^-_1$		4.019		−1.026
$9/2^-_1$		3.555		−0.850
$11/2^-_1$		4.441		−1.019
$13/2^-_1$		4.040		−0.994
^{212}At	Expt.	Calc.	Expt.	Calc.
1^-_1		+0.121		+0.121
2^-_1		+0.376		+0.226
3^-_1		+0.726		+0.195
15^-_1	9.46(8)	+7.367		−0.837
11^+_1	5.94(11)	+1.874		−0.971
11^+_2		+6.071		−1.081
^{214}At	Expt.	Calc.	Expt.	Calc.
1^-_1		+0.261		+0.120
2^-_1		+0.513		+0.186
3^-_1		+0.825		+0.344

μ_N in experiment and the theoretical result is $+1.874\,\mu_N$, which is 3.2 times smaller than the experimental data. The magnetic moment of the 11^+_2 state calculated at 1.417 MeV is $+6.071\,\mu_N$, which is very close to the experimental value. Thus the 11^+_1 and 11^+_2 states might be reversely calculated in energy compared to the experimentally observed states. In our calculation, the 11^+_2 state, which consists of the $(\nu g_{9/2} \otimes \pi h^2_{9/2} i_{13/2})$ configuration, is located 0.344 MeV higher than the 11^+_1 state.

E. Rn isotopes

Here $^{213-216}$Rn isotopes are discussed. Figure 18 shows the theoretical energy spectrum of ^{214}Rn in comparison with the experimental data [15,24]. The yrast band is well reproduced in our calculation. The spin-parity of the state observed at 1.332 MeV is not assigned (not shown in this figure). This state decays to the 2^+ state at 0.695 MeV. In our calculation, the 2^+_2 state is calculated at 1.626 MeV. Considering this result and the comparison with neighboring nuclei such as ^{212}Po and ^{216}Rn, the spin-parity of the experimental state at 1.332 MeV is inferred to be 2^+.

Figure 19 shows the theoretical energy spectrum of ^{216}Rn in comparison with the experimental data [15,32]. In ^{216}Rn the spin-parity of the state at 1.838 MeV is assigned as $(8^+,9^+,10^+)$. The 8^+_2, 9^+_1, and 10^+_2 states are calculated at 1.872, 2.217, and 2.369 MeV, respectively. Thus our calculation suggests that the spin-parity of the state at 1.838 MeV is 8^+. One of the peculiar features of even-even nuclei in this region is the narrow energy gap between the 6^+ and 8^+ states in the yrast band. In ^{216}Rn, however, the narrow energy gap between the 6^+ and 8^+ states is not seen anymore in experiment due to the evolution of quadrupole collectivity and the calculation reproduces this feature. Some characteristic features of ^{214}Rn and ^{216}Rn are analyzed and discussed in Sec. IV.

Figure 20 shows the theoretical energy spectrum of ^{213}Rn in comparison with the experimental data [15,21]. All the identified states are well reproduced. In ^{213}Rn, the $(25/2^+)$ state is observed at $1.664 + x$ MeV with x unknown. The $25/2^+_1$ state is calculated at 1.670 MeV. Our calculation shows that the ground $9/2^+_1$ state, the $11/2^+_1$ state at 0.622 MeV, and the $15/2^-_1$ state at 0.837 MeV, mainly consist of the $(\nu g_{9/2} \otimes \pi h^3_{9/2} f_{7/2})$, $(\nu i_{11/2} \otimes \pi h^3_{9/2} f_{7/2})$, and $(\nu j_{15/2} \otimes \pi h^3_{9/2} f_{7/2})$ configurations, respectively. These energies are very close to the single-particle energies for the neutron $1g_{9/2}$, $0i_{11/2}$, and $0j_{15/2}$ orbitals, which are given as 0.0 MeV, 0.579 MeV, and 0.783 MeV, respectively. This indicates that one valence neutron in the specific single-particle orbital determines nature of each state, namely, its spin and parity.

Figure 21 shows the theoretical energy spectrum of ^{215}Rn in comparison with the experimental data [15,30]. In ^{215}Rn,

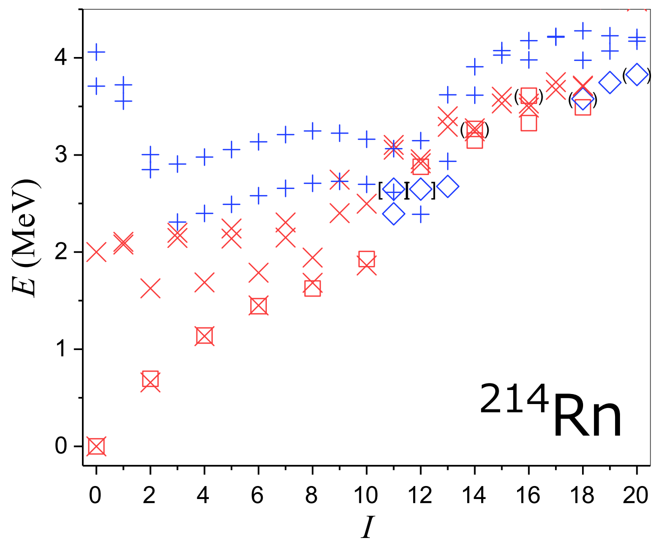

FIG. 18. Same as Fig. 4, but for ^{214}Rn. The experimental data are taken from Refs. [15,24].

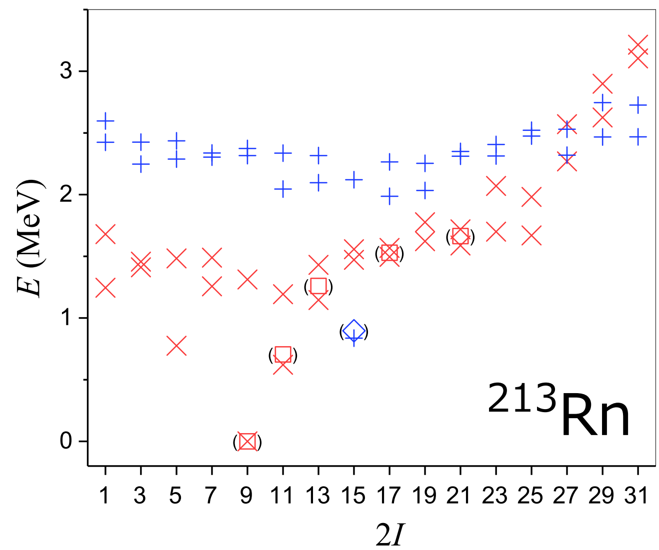

FIG. 20. Same as Fig. 1, but for ^{213}Rn. The experimental data are taken from Refs. [15,21].

the spin of the positive parity state observed at 0.214 MeV is assigned as $(7/2,9/2)^+$. The $7/2_1^+$ and $9/2_2^+$ states are calculated at 0.301 MeV and 0.795 MeV, respectively. Thus the spin of the state observed at 0.214 MeV is suggested as 7/2. The spin of the negative parity state observed at 0.291 MeV is assigned as $(7/2,9/2,11/2)^-$. However, the calculation predicts no negative parity states below 0.7 MeV. The $15/2_1^-$ state, which is not observed in experiment, is calculated at 0.733 MeV.

Calculated results for $B(E2)$ values and electromagnetic moments of Rn isotopes are given in Tables XII and XIII in comparison with the experimental data [15,21,24,30,32]. In ^{214}Rn, the observed $B(E2;6_1^+\to 4_1^+)$ and $B(E2;8_1^+\to 6_1^+)$ values are much smaller, whereas the calculation predicts large $B(E2)$ values. The magnetic moments of ^{213}Rn are well reproduced.

F. Fr isotopes

Here $^{214-217}$Fr isotopes are discussed. Figure 22 shows the theoretical energy spectrum of ^{215}Fr in comparison with the experimental data [15,30]. In ^{215}Fr, energy levels of low-lying negative parity states are well reproduced. A $(13/2^+)$ state is observed at 0.835 MeV in experiment. However, the $13/2_1^+$ state is calculated at 1.224 MeV, which is 0.409 MeV higher than the experimental one.

Figure 23 shows the theoretical energy spectrum of ^{217}Fr in comparison with the experimental data [15,33]. In ^{217}Fr,

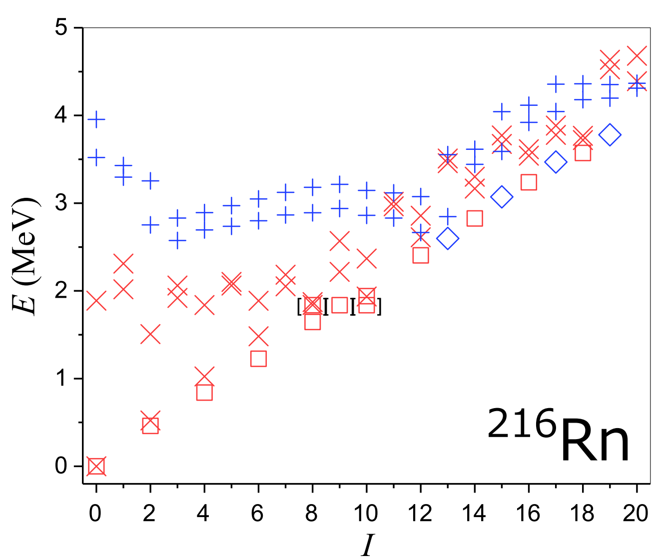

FIG. 19. Same as Fig. 4, but for ^{216}Rn. The experimental data are taken from Refs. [15,32].

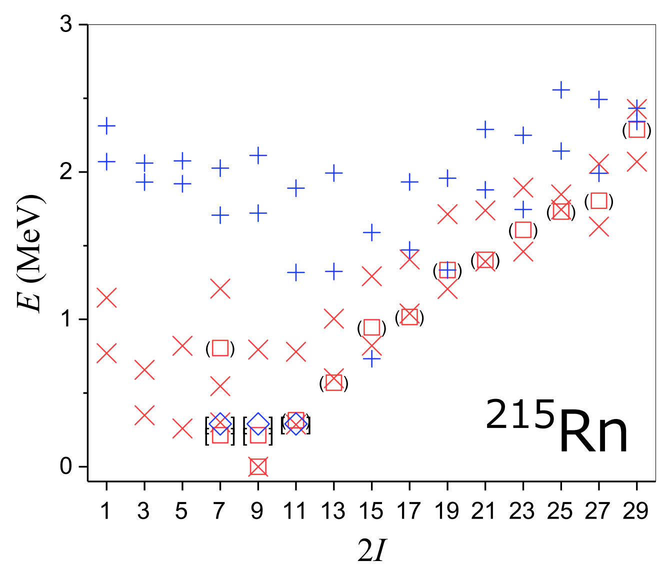

FIG. 21. Same as Fig. 4, but for ^{215}Rn. The experimental data are taken from Refs. [15,30].

TABLE XII. Same as Table III, but for Rn isotopes. The experimental data are taken from Refs. [15,21,24,30,32].

^{214}Rn	$B(E2)$	
	Expt.	Calc.
$2_1^+ \to 0_1^+$	>0.032	17.380
$4_1^+ \to 2_1^+$	>0.28	23.101
$6_1^+ \to 4_1^+$	3.8^{+17}_{-9}	21.614
$8_1^+ \to 6_1^+$	3.3^{+3}_{-1}	15.905
$10_1^+ \to 8_1^+$	2.9(7)	5.921
$12_1^+ \to 10_1^+$	>0.0064	4.820
$14_1^+ \to 12_1^+$		15.829
$16_1^+ \to 14_1^+$	$\leqslant 4.4(3)$	11.260
$18_1^+ \to 16_1^+$	0.71(5)	0.722
$13_1^- \to 11_1^-$	0.93(8)	0.099
^{216}Rn	Expt.	Calc.
$2_1^+ \to 0_1^+$		28.567
$4_1^+ \to 2_1^+$		40.613
$6_1^+ \to 4_1^+$		40.704
$8_1^+ \to 6_1^+$		9.671
$10_1^+ \to 8_1^+$		3.111
^{213}Rn	Expt.	Calc.
$7/2_1^+ \to 9/2_1^+$		3.676
$11/2_1^+ \to 9/2_1^+$		0.415
$13/2_1^+ \to 9/2_1^+$		8.619
$17/2_1^+ \to 13/2_1^+$		4.536
$21/2_1^+ \to 17/2_1^+$	1.68(16)	2.287
^{215}Rn	Expt.	Calc.
$7/2_1^+ \to 9/2_1^+$		18.315
$11/2_1^+ \to 9/2_1^+$		0.467
$13/2_1^+ \to 9/2_1^+$		22.646

TABLE XIII. Same as Table IV, but for Rn isotopes. The experimental data are taken from Refs. [15,21,24,30,32].

^{214}Rn	μ		Q	
	Expt.	Calc.	Expt.	Calc.
2_1^+		+0.449		−0.370
4_1^+		+0.378		−0.601
6_1^+		−0.248		−0.772
8_1^+		−0.969		−0.992
10_1^+		+0.135		−1.364
^{216}Rn	Expt.	Calc.	Expt.	Calc.
2_1^+		+0.612		−0.629
4_1^+		+1.021		−0.890
6_1^+		+1.138		−1.046
8_1^+		+5.923		−1.135
10_1^+		+0.236		−1.298
^{213}Rn	Expt.	Calc.	Expt.	Calc.
$5/2_1^+$		−1.955		−0.526
$7/2_1^+$		−0.892		−0.427
$9/2_1^+$		−1.293		−0.718
$11/2_1^+$		+1.285		−0.756
$21/2_1^+$	4.73(11)	+3.797		−0.880
$25/2_1^+$	7.63(25)	+5.367		−0.660
$15/2_1^-$		−1.373		−0.909
$31/2_1^-$	9.90(8)	+5.313		−0.796
^{215}Rn	Expt.	Calc.	Expt.	Calc.
$7/2_1^+$		−0.725		−0.636
$9/2_1^+$		−1.130		−0.700
$11/2_1^+$		+1.294		−1.136
$13/2_1^+$		−0.489		−0.820

the spins and parities of the states observed at 0.209 and 0.275 MeV are not assigned (not shown in this figure). The $7/2_1^-$, $7/2_2^-$, and $5/2_1^-$ states are calculated at 0.182, 0.342, and 0.462 MeV. Thus it is suggested that two of these states correspond to the experimental states at 0.209 and 0.275 MeV. The experimental energy levels of high-spin states, $13/2_1^-$, $15/2_1^-$, $17/2_1^-$, $21/2_1^-$, and $25/2_1^-$ states, are not reproduced well in comparison to other Fr isotopes. These states look like members of a quadrupole vibrational band on the ground 9_1^- state. In the present analysis of adjusting the two-body effective interactions, we have not included ^{217}Fr since it is a complicated system with five valence protons and two neutrons. The quadrupole-quadrupole interactions between like particles and/or the hexadecapole-hexadecapole interactions between a neutron and a proton might be necessary for a better reproduction.

Figure 24 shows the theoretical energy spectrum of ^{214}Fr in comparison with the experimental data [15,24]. In ^{214}Fr, low-lying negative parity states are well reproduced. The (8^-) state observed at 0.122 MeV is a spin-gap isomer with a half-life of 3.35(5) ms [15]. This state disintegrates only by the α-decay. The $0_1^-, 1_1^-, \ldots, 9_1^-$ states mainly consist of the $(\nu g_{9/2} \otimes \pi h_{9/2}^4 f_{7/2})$ configuration. The 6_1^-, 7_1^-, and 9_1^- states, which are connected to the 8_1^- state by $E2$ or $M1$ transitions, are calculated higher than the 8_1^- state. As mentioned above, the calculation reproduces the situation that the 9_1^- state is slightly higher than the 8_1^- state. The 9_1^- state is indeed unfavored in the $(\nu g_{9/2} \otimes \pi h_{9/2}^4 f_{7/2})$ configuration, in which at least one proton pair with angular momentum zero have to be broken in the $0h_{9/2}$ orbital. The $10_2^-, 11_1^-, 12_1^-, \ldots, 15_1^-$ states are admixtures of the $(\nu g_{9/2} \otimes \pi h_{9/2}^5)$ and $(\nu g_{9/2} \otimes \pi h_{9/2}^4 f_{7/2})$ configurations.

Figure 25 shows the theoretical energy spectrum of ^{216}Fr in comparison with the experimental data [15,32]. In ^{216}Fr, the spin-parity of the state observed at 0.142 MeV is assigned as $(0^-, 1^-, 2^-)$. The 0_1^-, 1_2^-, and 2_2^- states are calculated at 0, 0.129, and 0.172 MeV, respectively. Thus it is inferred that the spin-parity of the state at 0.142 MeV is 1^- or 2^-. The experimentally observed (9^-) state with an unknown energy is calculated at 0.117 MeV.

Calculated results for $B(E2)$ values and electromagnetic moments of Fr isotopes are given in Tables XIV and XV in comparison with the experimental data [15,24,30]. The

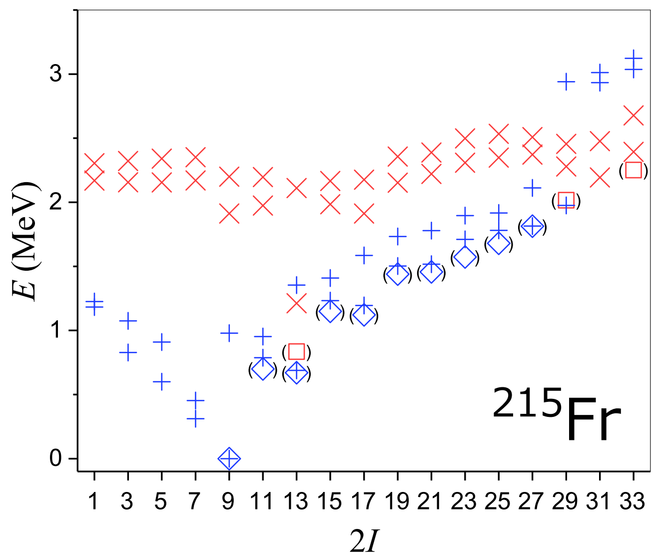

FIG. 22. Same as Fig. 1, but for ^{215}Fr. The experimental data are taken from Refs. [15,30].

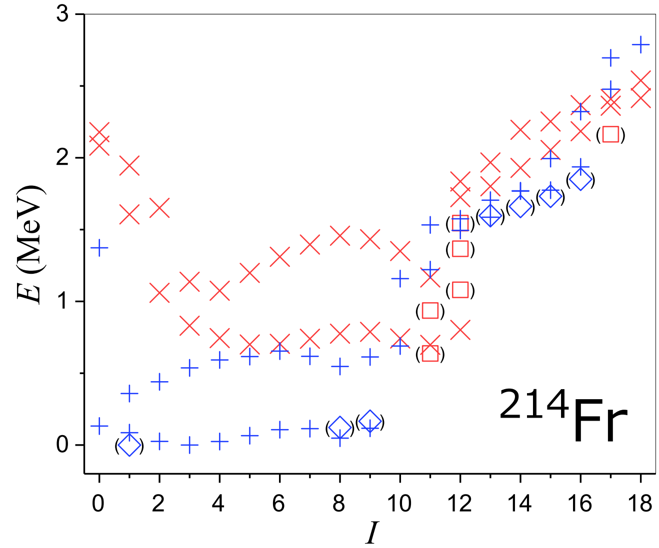

FIG. 24. Same as Fig. 1, but for ^{214}Fr. The experimental data are taken from Refs. [15,24].

experimental $B(E2; 19/2^-_1 \to 15/2^-_1)$ value of ^{215}Fr is 0.6(4) W.u. The calculated $B(E2)$ value of the same transition is 17.221 W.u., which is much larger than the experimental one. The $15/2^-_2$ state is calculated 0.181 MeV higher than the $15/2^-_1$ state. The $B(E2)$ value from the $19/2^-_1$ state to the $15/2^-_2$ state is calculated as 0.015 W.u. Therefore the calculated $15/2^-_1$ and $15/2^-_2$ states might be largely admixed. The electromagnetic moments are well reproduced except for the magnetic moment of the 11^+_1 state in ^{214}Fr. The magnetic moment of the 11^+_2 state is calculated as 2.982 μ_N. It is thus difficult to resolve the discrepancy even if the 11^+_1 and 11^+_2 states are reversely predicted in our calculation. However, it should be noted that the experimental 11^+ state is ambiguous with respect to spin and parity.

IV. DISCUSSION

In this section, structure of some even-even nuclei is investigated. The expectation numbers of pairs for the yrast states are calculated using the pair-truncated shell model (PTSM) [34–36]. In the present scheme, the building blocks are angular momenta zero (S), two (D), and four (G) collective pairs, and also noncollective (H) pairs. The S, D, and G pair-creation operators are defined as

$$S^\dagger = \sum_j \alpha_j A_0^{\dagger(0)}(jj), \tag{13}$$

$$D_M^\dagger = \sum_{j_1 j_2} \beta_{j_1 j_2} A_M^{\dagger(2)}(j_1 j_2), \tag{14}$$

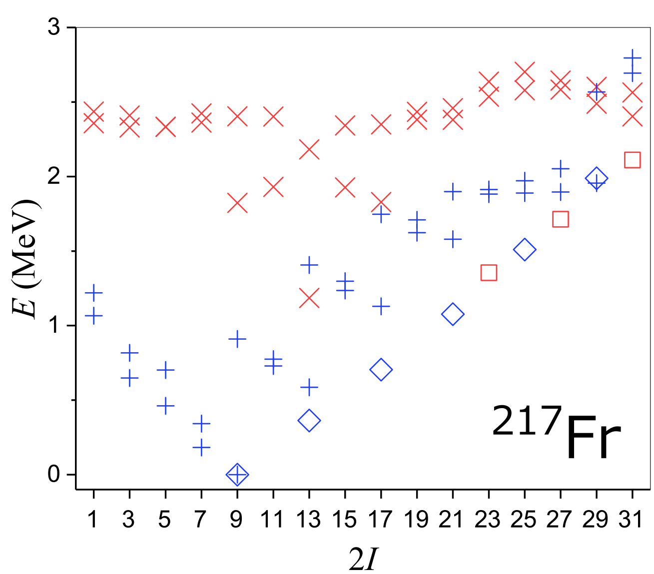

FIG. 23. Same as Fig. 1, but for ^{217}Fr. The experimental data are taken from Refs. [15,33].

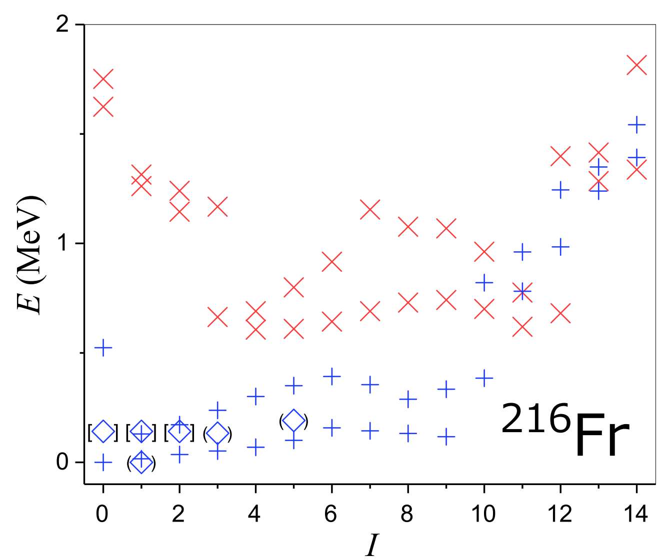

FIG. 25. Same as Fig. 4, but for ^{216}Fr. The experimental data are taken from Refs. [15,32].

TABLE XIV. Same as Table III, but for Fr isotopes. The experimental data are taken from Refs. [15,24,30].

^{215}Fr	$B(E2)$	
	Expt.	Calc.
$5/2_1^- \to 9/2_1^-$		16.474
$7/2_1^- \to 9/2_1^-$		3.610
$7/2_2^- \to 9/2_1^-$		20.475
$13/2_1^- \to 9/2_1^-$		17.350
$19/2_1^- \to 15/2_1^-$	0.6(4)	17.221
$19/2_1^- \to 15/2_2^-$		0.015
$23/2_1^- \to 19/2_1^-$	12(5)	14.100
$27/2_1^- \to 23/2_1^-$	1.1(8)	6.365
$27/2_2^- \to 23/2_1^-$		0.002
^{217}Fr	Expt.	Calc.
$5/2_1^- \to 9/2_1^-$		28.245
$7/2_1^- \to 9/2_1^-$		1.883
$7/2_2^- \to 9/2_1^-$		32.920
$13/2_1^- \to 9/2_1^-$		28.429
^{214}Fr	Expt.	Calc.
$5_1^- \to 3_1^-$		3.336
$8_1^- \to 9_1^-$		4.374
$15_1^- \to 13_1^-$	0.68(24)	0.221
^{216}Fr	Expt.	Calc.
$3_1^- \to 1_1^-$		1.372
$5_1^- \to 3_1^-$		5.789

TABLE XV. Same as Table IV, but for Fr isotopes. The experimental data are taken from Refs. [15,24,30].

^{215}Fr	μ		Q	
	Expt.	Calc.	Expt.	Calc.
$7/2_1^-$		+4.010		−0.664
$9/2_1^-$		+3.690		−0.183
$11/2_1^-$		+3.546		−0.329
$13/2_1^-$		+4.089		−0.366
$19/2_1^-$	3.1(9)	+2.560		−0.771
$23/2_1^-$	3.8(12)	+2.211		−1.001
^{217}Fr	Expt.	Calc.	Expt.	Calc.
$7/2_1^-$		+4.084		−0.878
$9/2_1^-$		+3.625		−0.464
$11/2_1^-$		+3.705		−0.627
$13/2_1^-$		+4.165		−0.577
^{214}Fr	Expt.	Calc.	Expt.	Calc.
1_1^-		+0.232		+0.119
8_1^-		+2.145		−0.610
9_1^-		+2.472		−0.608
14_1^-	+8.5(4)	+7.412		−0.318
14_2^-		+6.013		−1.339
11_1^+	+5.62(7)	+1.905	0.82(22)	−0.874
11_2^+		+2.982		−1.217
^{216}Fr	Expt.	Calc.	Expt.	Calc.
1_1^-		+0.275		+0.138
3_1^-		+0.743		+0.277
5_1^-		+1.414		−0.059

$$G_M^{\dagger} = \sum_{j_1 j_2} \gamma_{j_1 j_2} A_M^{\dagger(4)}(j_1 j_2), \quad (15)$$

where the pair creation operator of two nucleons in the orbitals j_1 and j_2 with total angular momentum J and magnetic quantum number M is constructed as

$$A_M^{\dagger(J)}(j_1 j_2) = [c_{j_1}^{\dagger} c_{j_2}^{\dagger}]_M^{(J)}. \quad (16)$$

The structure coefficients α, β, and γ are determined by variation.

The H pair creation operators for neutrons are defined as

$$H_{M\nu}^{\dagger(K)} = \begin{cases} [c_{j_{15/2}}^{\dagger} c_{j_{15/2}}^{\dagger}]_M^{(K)} & K = 0,2,4,\ldots,14, \\ [c_{g_{9/2}}^{\dagger} c_{g_{9/2}}^{\dagger}]_M^{(K)} & K = 0,2,4,6,8, \\ [c_{g_{9/2}}^{\dagger} c_{i_{11/2}}^{\dagger}]_M^{(K)} & K = 1,2,3,\ldots,10, \end{cases} \quad (17)$$

and those for protons are defined as

$$H_{M\pi}^{\dagger(K)} = \begin{cases} [c_{i_{13/2}}^{\dagger} c_{i_{13/2}}^{\dagger}]_M^{(K)} & K = 0,2,4,\ldots,12, \\ [c_{h_{9/2}}^{\dagger} c_{h_{9/2}}^{\dagger}]_M^{(K)} & K = 0,2,4,6,8, \\ [c_{h_{9/2}}^{\dagger} c_{f_{7/2}}^{\dagger}]_M^{(K)} & K = 1,2,3,\ldots,8. \end{cases} \quad (18)$$

Using the S, D, G, and H pair-creation operators, a many-body wave function of like nucleons can be constructed as

$$|\Psi(I\eta)\rangle = (S^{\dagger})^{n_s}(D^{\dagger})^{n_d}(G^{\dagger})^{n_g}(H^{\dagger})^{n_h}|-\rangle. \quad (19)$$

The number of valence nucleon pairs, $n_s + n_d + n_g + n_h$, is fixed for a specific nucleus. The Hamiltonian for this truncated space (PTSM space) is set identical to the present shell-model Hamiltonian. The consistency between the results with the two methods (SM and PTSM) was discussed concerning the energy levels of the ^{82}Se nucleus up to 6 MeV in Ref. [37]. In Ref. [38] the energy levels of the ^{208}Rn nucleus up to 3.5 MeV in the SM are compared with those in the PTSM. The good correspondence between the SM and the PTSM is seen.

Figure 26 shows the expectation numbers of pairs for the yrast states up to spin 10 in ^{212}Po. This nucleus is a system with two neutrons and two protons outside the doubly magic core ^{208}Pb. It is seen that the proton wave function mainly consists of the S pair, and the contributions from the D pair and the G pair are small for all the spins. The maximum contribution except from the S pair is 0.357 pairs of the D pair in the 2_1^+ state. Thus the total excitation is mainly determined by the neutron part. Up to the 8_1^+ state, the states consist of the $(\nu g_{9/2})^2_{I^+}$ ($I = 0,2,\ldots,8$) configuration. One neutron needs to be excited to the $0i_{11/2}$ orbital to make the 10_1^+ state since the maximum spin of two neutrons in the $1g_{9/2}$ orbital is eight. Therefore, the 10_1^+ state consists of the $(\nu g_{9/2} i_{11/2})_{10^+}$ configuration. In this mass region, the strength of the neutron monopole pairing is smaller than that of protons. Thus the configuration mixing of neutrons is preferred.

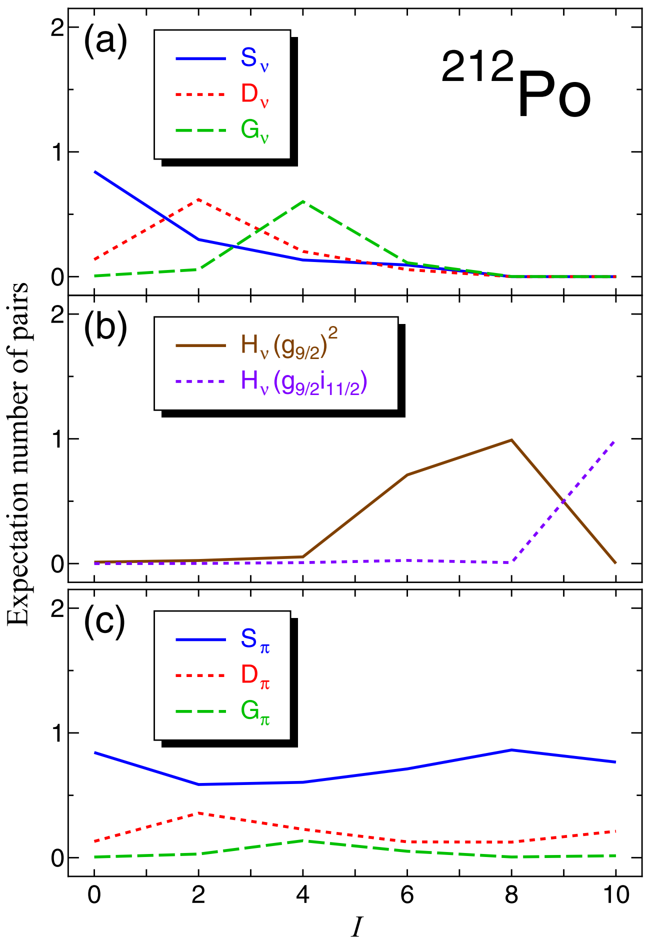

FIG. 26. (a) The neutron expectation numbers of collective pairs for ^{212}Po. The S, D, and G indicate S pair, D pair, and G pair, respectively. (b) The neutron expectation numbers of non-collective $(g_{9/2})^2$ pair $[(g_{9/2})^2]$ and $g_{9/2}i_{11/2}$ pair $(g_{9/2}i_{11/2})$. The definitions of noncollective pairs are given in the text. (c) The proton expectation numbers of collective pairs for ^{212}Po.

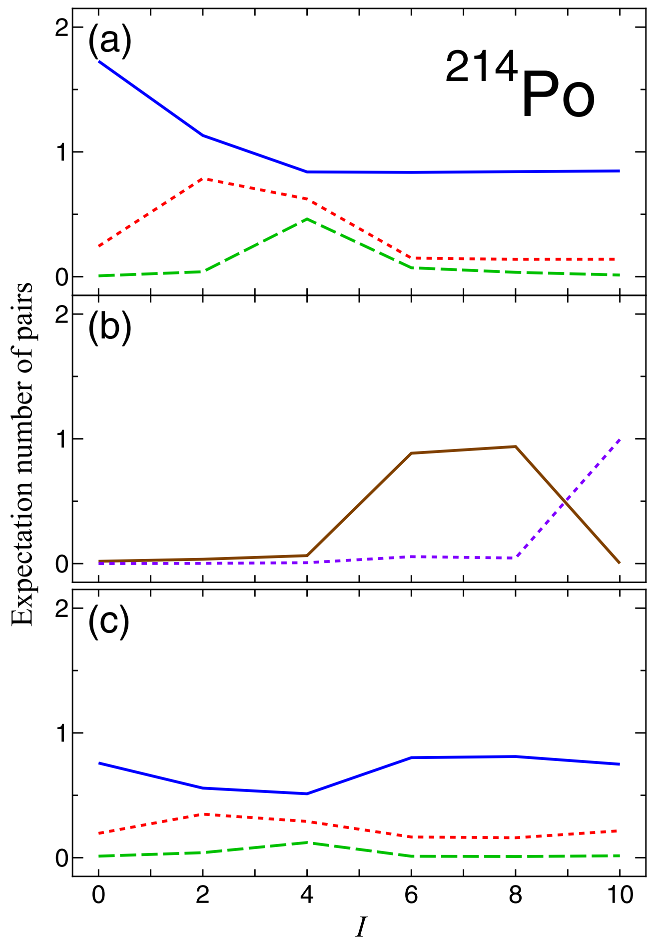

FIG. 27. The same as Fig. 26, but for ^{214}Po.

Figure 27 shows the expectation numbers of pairs for the yrast states up to spin 10 in ^{214}Po. This nucleus is a system with four neutrons and two protons outside the ^{208}Pb core. Similar to ^{212}Po, the proton part mainly consists of the S pair for all the spins. For the neutron part, the ground state consists of two neutron S pairs. For the $I^\pi = 2_1^+$, 6_1^+, 8_1^+, and 10_1^+ states, two neutrons are coupled to the S pair, and the other two neutrons are coupled to pairs with spin I. For the 2_1^+ state, the expectation numbers of the neutron D pair and the proton D pair are 0.787 and 0.349, respectively. This result means that the 2_1^+ state mainly consists of the neutron D pair. For the 4_1^+ state, the expectation numbers of the neutron D pair, the neutron G pair, and the proton D pair are 0.623, 0.462, and 0.291, respectively. Thus it is inferred that the 4_1^+ state consists of mixtures of two types of pair structures. The first one consists of one neutron S pair, one neutron D pair, and one proton D pair, which are coupled with spin 4 $[S_\nu(D_\nu D_\pi)_{4^+}]$. The second one consists of one neutron S pair, one neutron G pair, and one proton S pair $(S_\nu G_\nu S_\pi)$.

Figure 28 shows the expectation numbers of pairs for the yrast states (except 6^+ and 8^+) in ^{214}Rn. Those numbers for the 6_2^+ and 8_2^+ states are shown instead of those for the 6_1^+ and 8_1^+ states, which are reversely reproduced in order in the PTSM calculations, compared to those in the SM calculations. This nucleus is a system with two neutrons and four protons outside the ^{208}Pb core. For all the spins, four protons are coupled to the S pairs and the spins are mainly determined by the neutron part. Similar to ^{212}Po, the yrast states up to spin 8 consist of the $(\nu g_{9/2})^2_{I^+}$ configuration and the 10_1^+ state consists of the $(\nu g_{9/2}i_{11/2})_{10^+}$ configuration.

Figure 29 shows the expectation numbers of pairs for the yrast states in ^{216}Rn. This nucleus is a system with four neutrons and four protons outside the ^{208}Pb core. Similar to the other three even-even nuclei, ^{212}Po, ^{214}Po, and ^{214}Rn, the ground state consists of two neutron S pairs and two proton S pairs, and the 2_1^+ state mainly consists of one neutron S pair, one neutron D pair, and two proton S pairs. For the 4_1^+ state, the expectation numbers of the neutron D pair, the neutron G pair, and the proton D pair are 0.810, 0.330, and 0.582, respectively. The 4_1^+ state has a similar structure with the 4_1^+ state in ^{214}Po. The structure of the 6_1^+ state, however, is different from the other three nuclei. The expectation numbers of the neutron D pair, the neutron G pair, and the neutron $(g_{9/2})^2_{6^+}$ pair are 0.811,

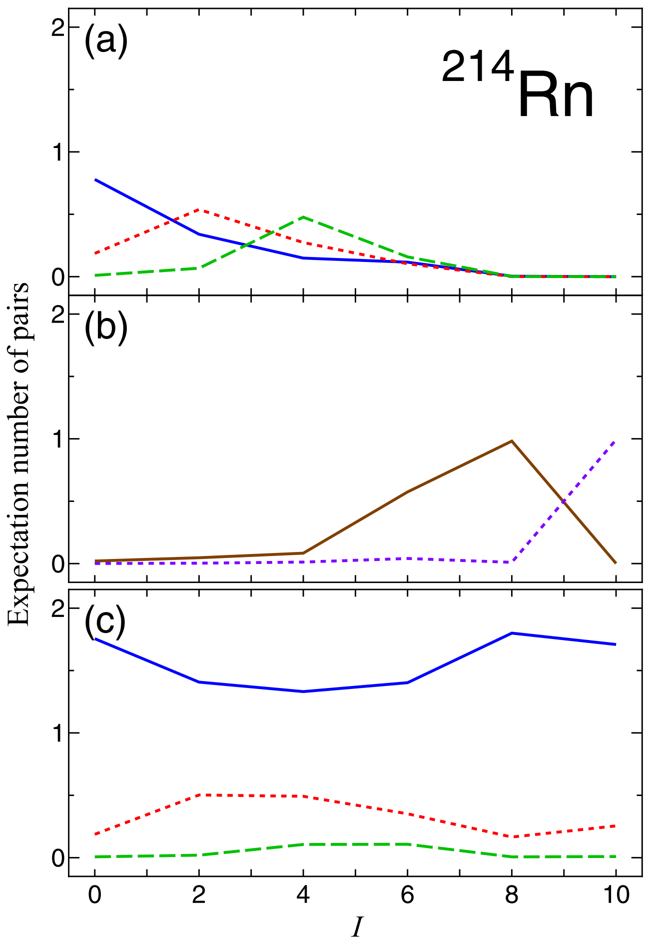

FIG. 28. The same as Fig. 26, but for ^{214}Rn.

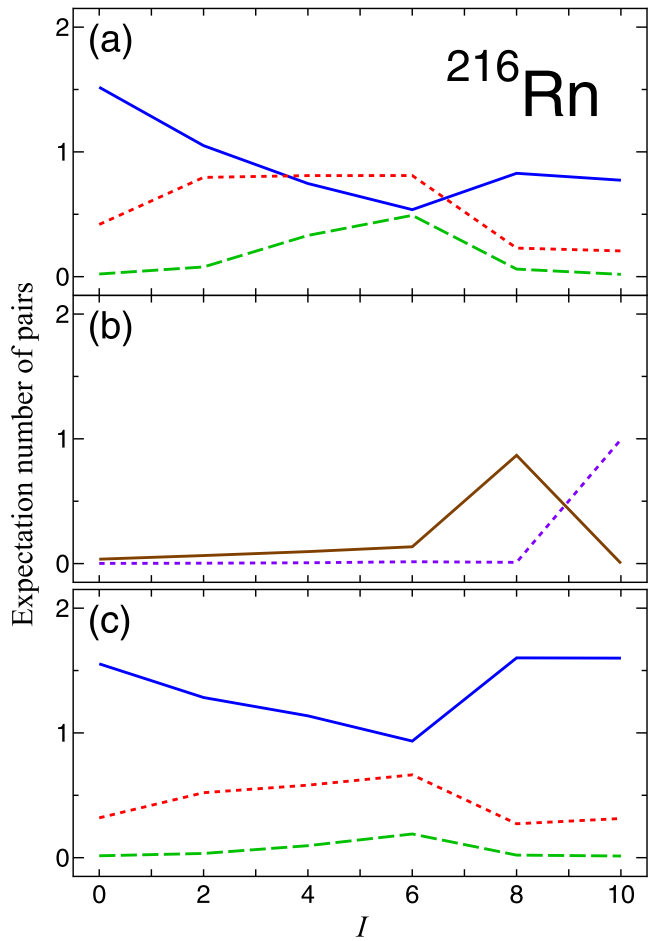

FIG. 29. The same as Fig. 26, but for ^{216}Rn.

0.492, and 0.135, respectively. The expectation number of the neutron $(g_{9/2})^2_{6^+}$ pair is small and that of the neutron D pair is large compared to the other three nuclei. This indicates that the nucleus shows an aspect of a collective feature.

Structure in low-lying states of nuclei with a few valence nucleons outside the doubly magic core ^{208}Pb is generally determined by the single-particle motion of the valence nucleons. However, as the number of valence nucleons increases, collective features appear. The collectivity of ^{216}Rn is also seen in the energy spectrum as discussed in Sec. III E.

A specific feature of even-even nuclei in this mass region is the narrow energy gap between the 6^+_1 and 8^+_1 states (e.g., see ^{210}Pb in Fig. 1). This small energy gap occurs due to the alignment of two neutrons. In this mass region, the yrast states up to spin 8 in even-even nuclei consist of the two neutrons in the $1g_{9/2}$ orbital. In the 8^+_1 state, the spin of two neutrons in the $1g_{9/2}$ orbital is stretched and the energy of the 8^+_1 state is lowered. However, the narrow energy gap between the 6^+_1 and 8^+_1 states is not seen in ^{216}Rn anymore (see Fig. 19).

V. SUMMARY

In the present study, the large-scale shell-model calculations have been carried out for even-even, odd-mass, and doubly odd nuclei of $_{82}$Pb, $_{83}$Bi, $_{84}$Po, $_{85}$At, $_{86}$Rn, and $_{87}$Fr isotopes in the neutron-rich region around the double magic ^{208}Pb nucleus.

For neutron single-particle levels, seven orbitals above the magic number 126, $1g_{9/2}$, $0i_{11/2}$, $0j_{15/2}$, $2d_{5/2}$, $3s_{1/2}$, $1g_{7/2}$, and $2d_{3/2}$ orbitals, have been taken into account. For proton single-particle levels, all the six orbitals in the major shell between the magic numbers 82 and 126, $0h_{9/2}$, $1f_{7/2}$, $0i_{13/2}$, $2p_{3/2}$, $1f_{5/2}$, and $2p_{1/2}$ orbitals, have been taken into account. The particle number dependence of the single-particle energies of the neutron $0j_{15/2}$ and $0i_{11/2}$ orbitals and the proton $0i_{13/2}$ and $1f_{7/2}$ orbitals have been assumed. They are changed linearly so as to reproduce the energy levels of low-lying states of the odd-mass nuclei. As for the effective two-body interaction, higher multipole-pairing interactions among like nucleons and the quadrupole-quadrupole interaction between neutrons and protons are employed in addition to the conventional pairing interactions. Only one set of the strengths of the two-body interactions has been adopted in all the nuclei considered.

Energy spectra, $E2$ transition rates, magnetic moments, and electric quadrupole moments have been calculated and compared with experimental data. Good agreements with the experimental data have been obtained not only for even-even and odd-mass nuclei, but also for doubly odd nuclei. Comparing our results and the experimental data, spins and parities of experimentally ambiguous states have been suggested.

Nine isomeric states are analyzed in terms of the shell-model configurations. Four isomeric states appearing in this region are classified as the spin-gap isomers, which do not take γ transitions with low-spin changes, such as $E2$ or $M1$ transitions, because of the large spin difference between initial and final states. The other five states become isomers even if they decay by the $E2$ transition. They become isomers since the energy gaps between the initial and final states are small.

ACKNOWLEDGMENTS

This work was supported by Grant-in-Aid for Scientific Research (C) (Grants No. 16K05341 and No. 17K05450) from Japan Society for the Promotion of Science (JSPS) and also by a Grant-in-Aid for JSPS Fellows (Grant No. 2610429).

[1] L. Chen, P. M. Walker, H. Geissel, Y. A. Litvinov, K. Beckert, P. Beller, F. Bosch, D. Boutin, L. Caceres, J. J. Carroll, D. M. Cullen, I. J. Cullen, B. Franzke, J. Gerl, M. Górska, G. A. Jones, A. Kishada, R. Knöbel, C. Kozhuharov, J. Kurcewicz, S. A. Litvinov, Z. Liu, S. Mandal, F. Montes, G. Münzenberg, F. Nolden, T. Ohtsubo, Z. Patyk, W. R. Plaß, Z. Podolyák, S. Rigby, N. Saito, T. Saito, C. Scheidenberger, E. C. Simpson, M. Shindo, M. Steck, B. Sun, S. J. Williams, H. Weick, M. Winkler, H.-J. Wollersheim, and T. Yamaguchi, Phys. Rev. Lett. **110**, 122502 (2013).

[2] A. Astier and M.-G. Porquet, Phys. Rev. C **83**, 034302 (2011).

[3] G. Lane, K. Maier, A. Byrne, G. Dracoulis, R. Broda, B. Fornal, M. Carpenter, R. Clark, M. Cromaz, R. Janssens, A. Macchiavelli, I. Wiedenhover, and K. Vetter, Phys. Lett. B **606**, 34 (2005).

[4] G. Lane, R. Broda, B. Fornal, A. Byrne, G. Dracoulis, J. Blomqvist, R. Clark, M. Cromaz, M. Deleplanque, R. Diamond, P. Fallon, R. Janssens, I. Lee, A. Macchiavelli, K. Maier, M. Rejmund, F. Stephens, C. Svensson, K. Vetter, D. Ward, I. Wiedenhover, and J. Wrzesinski, Nucl. Phys. A **682**, 71 (2001).

[5] P. Mello and J. Flores, Nucl. Phys. **47**, 177 (1963).

[6] Y. E. Kim and J. O. Rasmussen, Nucl. Phys. **47**, 184 (1963).

[7] G. Herling and T. Kuo, Nucl. Phys. A **181**, 113 (1972).

[8] P. Alexa, J. Kvasil, N. V. Minh, and R. K. Sheline, Phys. Rev. C **55**, 179 (1997).

[9] L. Coraggio, A. Covello, A. Gargano, and N. Itaco, Phys. Rev. C **76**, 061303 (2007).

[10] L. W. Nordheim, Rev. Mod. Phys. **23**, 322 (1951).

[11] P. Alexa and R. K. Sheline, Phys. Rev. C **56**, 3087 (1997).

[12] C. W. Ma and W. W. True, Phys. Rev. C **8**, 2313 (1973).

[13] E. Teruya, K. Higashiyama, and N. Yoshinaga, Phys. Rev. C **93**, 064327 (2016).

[14] E. Teruya, N. Yoshinaga, K. Higashiyama, and A. Odahara, Phys. Rev. C **92**, 034320 (2015).

[15] Evaluated Nuclear Structure Data File (ENSDF), www.nndc.bnl.gov/ensdf/.

[16] M. S. Basunia, Nucl. Data Sheets **121**, 561 (2014).

[17] E. Browne, Nucl. Data Sheets **104**, 427 (2005).

[18] B. Singh, D. Abriola, C. Baglin, V. Demetriou, and T. Johnson, Nucl. Data Sheets **114**, 661 (2013).

[19] I. Hamamoto, Nucl. Phys. A **155**, 362 (1970).

[20] E. Flynn, G. Igo, R. Broglia, S. Landowne, V. Paar, and B. Nilsson, Nucl. Phys. A **195**, 97 (1972).

[21] M. S. Basunia, Nucl. Data Sheets **108**, 633 (2007).

[22] A. Astier, P. Petkov, M.-G. Porquet, D. S. Delion, and P. Schuck, Phys. Rev. Lett. **104**, 042701 (2010).

[23] A. Astier, P. Petkov, M.-G. Porquet, D. S. Delion, and P. Schuck, Eur. Phys. J. A **46**, 165 (2010).

[24] S.-C. Wu, Nucl. Data Sheets **110**, 681 (2009).

[25] Y. Suzuki and S. Ohkubo, Phys. Rev. C **82**, 041303 (2010).

[26] D. S. Delion, R. J. Liotta, P. Schuck, A. Astier, and M. G. Porquet, Phys. Rev. C **85**, 064306 (2012).

[27] H. W. Taylor, B. Singh, and D. A. Viggars, Phys. Rev. C **34**, 2322 (1986).

[28] D. Kocheva, G. Rainovski, J. Jolie, N. Pietralla, A. Blazhev, R. Altenkirch, S. Ansari, A. Astier, M. Bast, M. Beckers *et al.*, Phys. Rev. C **96**, 044305 (2017).

[29] M. D. Seliverstov, T. E. Cocolios, W. Dexters, A. N. Andreyev, S. Antalic, A. E. Barzakh, B. Bastin, J. Büscher, I. G. Darby, D. V. Fedorov, V. N. Fedosseev, K. T. Flanagan, S. Franchoo, G. Huber, M. Huyse, M. Keupers, U. Köster, Y. Kudryavtsev, B. A. Marsh, P. L. Molkanov, R. D. Page, A. M. Sjödin, I. Stefan, P. Van Duppen, M. Venhart, and S. G. Zemlyanoy, Phys. Rev. C **89**, 034323 (2014).

[30] B. Singh, Nucl. Data Sheets **114**, 2023 (2013).

[31] C. F. Liang, P. Paris, and R. K. Sheline, Phys. Rev. C **47**, 1801 (1993).

[32] S.-C. Wu, Nucl. Data Sheets **108**, 1057 (2007).

[33] Y. A. Akovali, Nucl. Data Sheets **100**, 141 (2003).

[34] N. Yoshinaga and K. Higashiyama, Phys. Rev. C **69**, 054309 (2004).

[35] K. Higashiyama and N. Yoshinaga, Phys. Rev. C **83**, 034321 (2011).

[36] K. Higashiyama and N. Yoshinaga, Phys. Rev. C **88**, 034315 (2013).

[37] N. Yoshinaga, K. Higashiyama, and P. H. Regan, Phys. Rev. C **78**, 044320 (2008).

[38] K. Higashiyama and N. Yoshinaga, in *EPJ Web of Conferences* (EDP Sciences, Les Ulis, 2014), Vol. 66, p. 02050.